Figure 3.124: Diagram of NMR tube with inserted coaxial reference insert. Image Courtesy of Wilmad-LabGlass; All Rights Reserved.

Another way to reference an NMR spectrum is to use a 85% H_3PO_4 standard sample. These can be prepared in the laboratory or purchased commercially. To allow for long term use, these samples are typically vacuum sealed, as opposed to capped the way NMR samples typically are. The procedure for using a separate reference is as follows.

1. Insert NMR sample tube into spectrometer.
2. Tune the ^{31}P probe and shim the magnetic field according to your individual instrument procedure.
3. Remove NMR sample tube and insert H_3PO_4 reference tube into spectrometer.
4. Begin NMR experiment. As scans proceed, perform a fourier transform and set the phosphorus signal to 0 ppm. Continue to reference spectrum until the shift stops changing.
5. Stop experiment.
6. Remove H_3PO_4 reference tube and insert NMR sample into spectrometer.
7. Run NMR experiment without changing the referencing of the spectrum.

3.7.4.5 ^{31}P NMR applications

3.7.4.5.1 Assaying sample purity

^{31}P NMR spectroscopy gives rise to single sharp peaks that facilitate differentiating phosphorus-containing species, such as starting materials from products. For this reason, ^{31}P NMR is a quick and simple technique for assaying sample purity. Beware, however, that a "clean" ^{31}P spectrum does not necessarily suggest a pure compound, only a mixture free of phosphorus-containing contaminants.

^{31}P NMR can also be used to determine the optical purity of a chiral sample. Adding an enantiomer to the chiral mixture to form two different diastereomers will give rise to two unique chemical shifts in the ^{31}P spectrum. The ratio of these peaks can then be compared to determine optical purity.

3.7.4.5.2 Monitoring reactions

As suggested in the previous section, ^{31}P NMR can be used to monitor a reaction involving phosphorus compounds. Consider the reaction between a slight excess of organic diphosphine ligand and a nickel(0)

bis-cyclooctadiene, (3.11).

<div align="right">(3.11)</div>
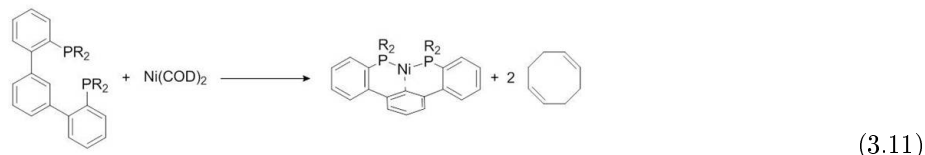
The reaction can be followed by ^{31}P NMR by simply taking a small aliquot from the reaction mixture and adding it to an NMR tube, filtering as needed. The sample is then used to acquire a ^{31}P NMR spectrum and the procedure can be repeated at different reaction times. The data acquired for these experiments is found in Figure 3.125. The changing in ^{31}P peak intensity can be used to monitor the reaction, which begins with a single signal at -4.40 ppm, corresponding to the free diphosphine ligand. After an hour, a new signal appears at 41.05 ppm, corresponding the the diphosphine nickel complex. The downfield peak grows as the reaction proceeds relative to the upfield peak. No change is observed between four and five hours, suggesting the conclusion of the reaction.
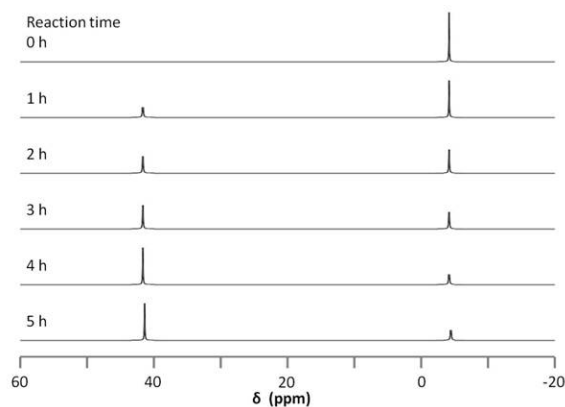

Figure 3.125: ^{31}P-{^{1}H} NMR spectra of the reaction of diphosphine ligand with nickel(0) *bis*-cyclooctadiene to make a diphosphine nickel complex over time.

There are a number of advantages for using ^{31}P for reaction monitoring when available as compared to ^{1}H NMR:

- There is no need for a deuterated solvent, which simplifies sample preparation and saves time and resources.
- The ^{31}P spectrum is simple and can be analyzed quickly. The corresponding ^{1}H NMR spectra for the above reaction would include a number of overlapping peaks for the two phosphorus species as well as peaks for both free and bound cyclooctadiene ligand.
- Purification of product is also easy assayed.

^{31}P NMR does not eliminate the need for ^{1}H NMR chacterization, as impurities lacking phosphorus will not appear in a ^{31}P experiment. However, at the completion of the reaction, both the crude and purified products can be easily analyzed by both ^{1}H and ^{31}P NMR spectroscopy.

3.7.4.5.3 Measuring epoxide content of carbon nanomaterials.

One can measure the amount of epoxide on nanomaterials such as carbon nanotubes and fullerenes by monitoring a reaction involving phosphorus compounds in a similar manner to that described above. This technique uses the catalytic reaction of methyltrioxorhenium ((3.12)). An epoxide reacts with methyltrioxorhenium to form a five membered ring. In the presence of triphenylphosphine (PPH_3), the catalyst is regenerated, forming an alkene and triphenylphosphine oxide ($OPPh_3$). The same reaction can be applied to carbon nanostructures and used to quantify the amount of epoxide on the nanomaterial. (3.13) illustrates the quantification of epoxide on a carbon nanotube.

$$(3.12)$$

$$(3.13)$$
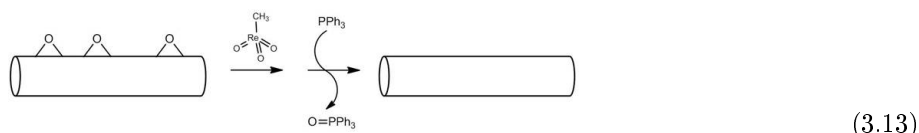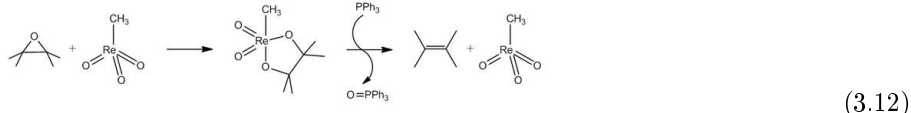
Because the amount of initial PPh_3 used in the reaction is known, the relative amounts of PPh_3 and $OPPh_3$ can be used to stoichiometrically determine the amount of epoxide on the nanotube. ^{31}P NMR spectroscopy is used to determine the relative amounts of PPh_3 and $OPPh_3$ (Figure 3.126).
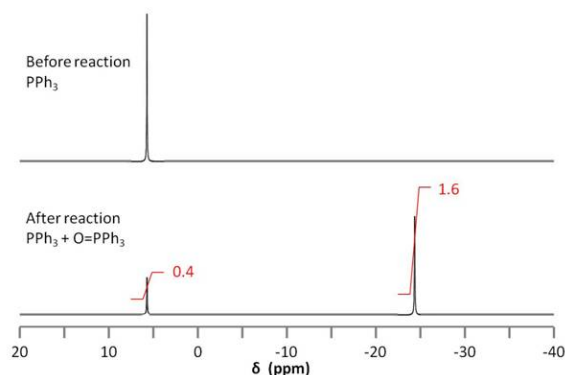

Figure 3.126: ^{31}P spectrum of experiment before addition of Re complex (top) and at the completion of experiment (bottom).

The integration of the two ^{31}P signals is used to quantify the amount of epoxide on the nanotube according to (3.14).

$$\text{Moles of epoxide} = \frac{\text{area of OPPh}_3\text{ peak}}{\text{area of PPh}_3\text{ peak}} \times \text{ moles PPh}_3$$

$$(3.14)$$

Thus, from a known quantity of PPh_3, one can find the amount of $OPPh_3$ formed and relate it stoichiometrically to the amount of epoxide on the nanotube. Not only does this experiment allow for such quantification, it is also unaffected by the presence of the many different species present in the experiment. This is because the compounds of interest, PPh_3 and $OPPh_3$, are the only ones that are characterized by ^{31}P NMR spectroscopy.

3.7.4.6 Conclusion

^{31}P NMR spectroscopy is a simple technique that can be used alongside ^{1}H NMR to characterize phosphorus-containing compounds. When used on its own, the biggest difference from ^{1}H NMR is that there is no need to utilize deuterated solvents. This advantage leads to many different applications of ^{31}P NMR, such as assaying purity and monitoring reactions.

3.7.4.7 Bibliography

- K. J. Coskran and J. G. Verkade, *Inorg. Chem.*, 1965, **4**, 1655.
- M. M. Crutchfield, C. H. Dungan, J. H. Letcher, V. Mark, and J. R. Van Wazer, *P31: Nuclear Magnetic Resonance*. Interscience, NY (1967).
- W. Guo, K. F. Kelly, A. R. Barron and W. E. Billups, *J. Am. Chem. Soc.*, 2008, **130**, 5414.
- K. Moedritzer, *J. Inorg. Nucl. Chem.*, 1961, **22**, 19.
- D. Ogrin, J. Chattopadhyay, A. K. Sadana, E. Billups, and A. R. Barron, *J. Am. Chem. Soc.*, 2006, **128**, 11322.
- K. J. Packer, *J. Chem. Soc.*, 1963, 960.
- J. G. Verkade, and L. D. Quin. *Phosphorus-31 NMR Spectroscopy in Stereochemical Analysis*. VCH, Deerfield Beach, FL (1987).

3.7.5 NMR Spectroscopy of Stereoisomers[23]

3.7.5.1 Introduction

Nuclear magnetic resonance (NMR) spectroscopy is a very useful tool used widely in modern organic chemistry. It exploits the differences in the magnetic properties of different nuclei in a molecule to yield information about the chemical environment of the nuclei, and subsequently the molecule, in question. NMR analysis lends itself to scientists more easily than say the more cryptic data achieved form ultraviolet or infared spectra because the differences in magnetic properties lend themselves to scientists very well. The chemical shifts that are characteristic of different chemical environments and the multiplicity of the peaks fit well with our conception of the way molecules are structured.

Using NMR spectroscopy, we can differentiate between constitutional isomers, stereoisomers, and enantiomers. The later two of these three classifications require close examination of the differences in NMR spectra associated with changes in chemical environment due to symmetry differences; however, the differentiation of constitutional isomers can be easily obtained.

3.7.5.2 Constitutional isomerism

Nuclei both posses charge and spin, or angular momentum, and from basic physics we know that a spinning charge generates a magnetic moment. The specific nature of this magnetic moment is the main concern of NMR spectroscopy.

For proton NMR, the local chemical environment makes different protons in a molecule resonate at different frequencies. This difference in resonance frequencies can be converted into a chemical shift (δ) for each nucleus being studied. Because each chemical environment results in a different chemical shift, one can easily assign peaks in the NMR data to specific functional groups based upon president. Presidents for chemical shifts can be found in any number of basic NMR text. For example, Figure 3.127 shows the spectra of ethyl formate and benzyl acetate. In the lower spectra, benzyl acetate, notice peaks at $\delta = 1.3$, 4.2, and 8.0 ppm characteristic of the primary, secondary, and aromatic protons, respectively, present in the molecule. In the spectra of ethyl formate (Figure 3.127b), notice that the number of peaks is is the same as that of benzyl acetate (Figure 3.127a); however, the multiplicity of peaks and their shifts is very different.

---

[23]This content is available online at <http://cnx.org/content/m38355/1.1/>.
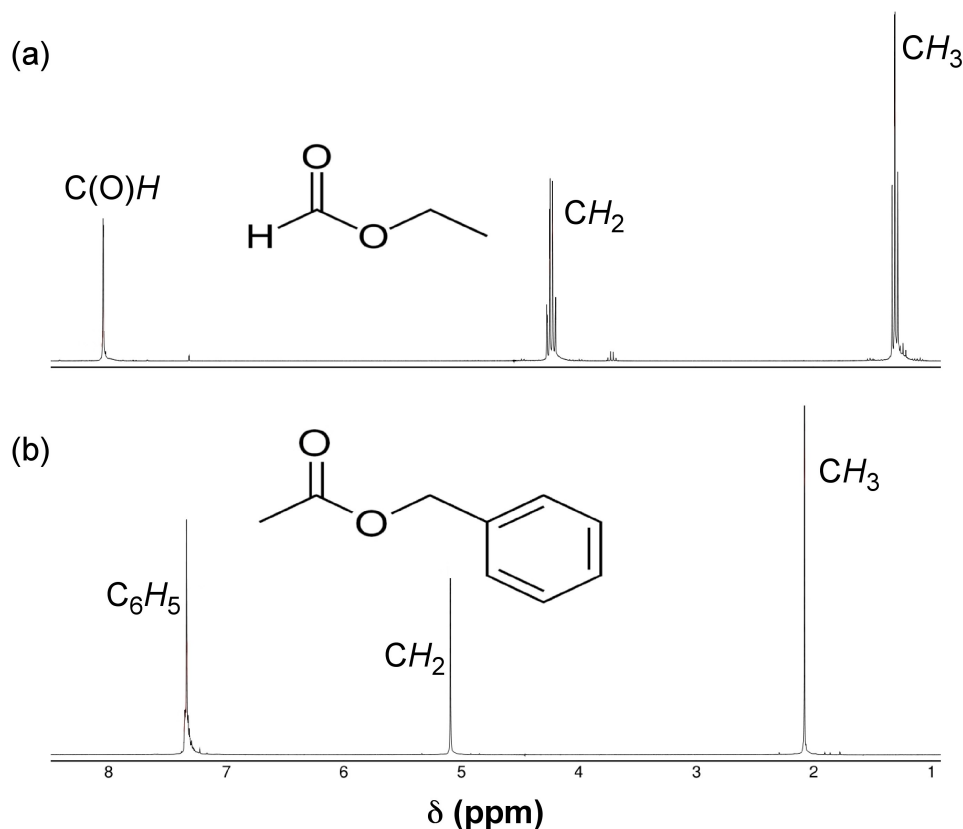
Figure 3.127: ^{1}H NMR spectra of (a) ethyl formate and (b) benzyl acetate.

The difference between these two spectra is due to geminal spin-spin coupling. Spin-spin coupling is the result of magnetic interaction between individual protons transmitted by the bonding electrons between the protons. This spin-spin coupling results in the speak splitting we see in the NMR data. One of the benefits of NMR spectroscopy is the sensitivity to very slight changes in chemical environment.

3.7.5.3 Stereoisomerism

3.7.5.3.1 Diastereomers

Based on their definition, diastereomers are stereoisomers that are not mirror images of each other and are not superimposable. In general, diastereomers have differing reactivity and physical properties. One common example is the difference between threose and erythrose (Figure 3.128).
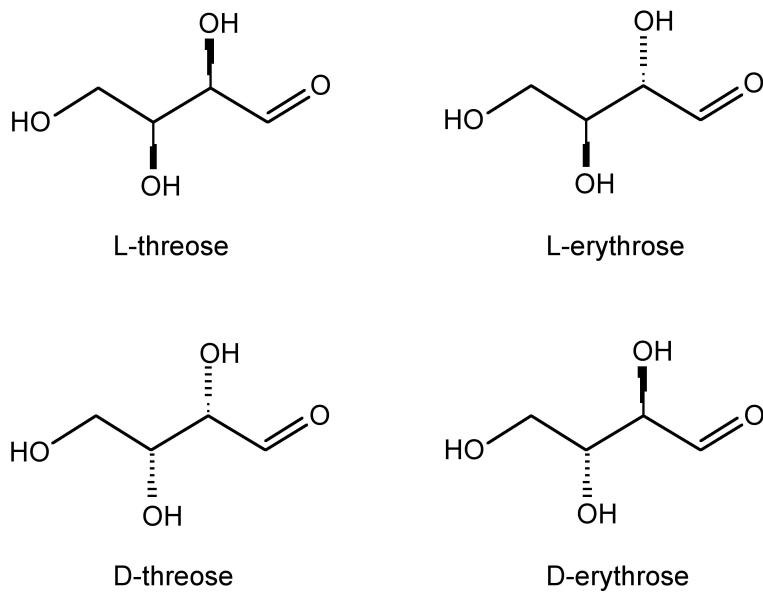
Figure 3.128: The structures of threose and erythrose.

As one can see from Figure 3.128, these chemicals are very similar each having the empirical formula of $C_4H_7O_4$. One may wonder: how are these slight differences in chemical structure represented in NMR? To answer this question, we must look at the Newman projections for a molecule of the general structure (Figure 3.129).
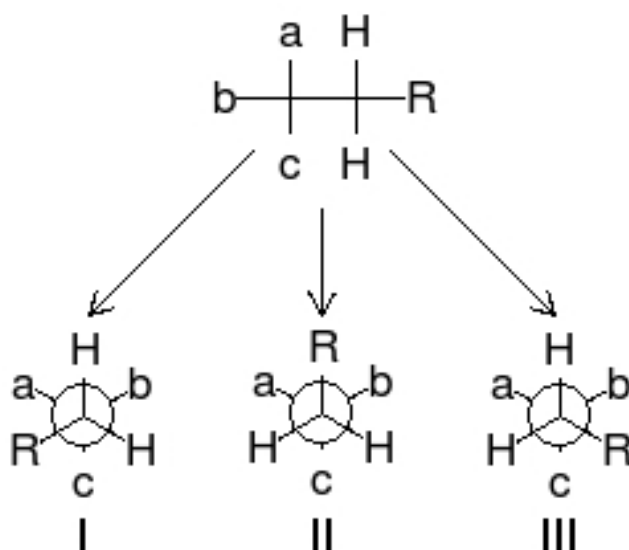
Figure 3.129: Newman projections of a general diastereomer.

One can easily notice that the two protons represented are always located in different chemical environments. This is true because the R group makes the proton resonance frequencies $v_1(I) \neq v_2(III)$, $v_2(I) \neq v_1(II)$, and $v_2(II) \neq v_1(III)$. Thus, diastereomers have different vicinal proton-proton couplings and the resulting chemical shifts can be used to identify the isomeric makeup of the sample.

3.7.5.3.2 Enantiomers

Enantiomers are compounds with a chiral center. In other words, they are non-superimposable mirror images. Unlike diastereomers, the only difference between enantiomers is their interaction with polarized light. Unfortunately, this indistinguishability of racemates includes NMR spectra. Thus, in order to differentiate between enantiomers, we must make use of an optically active solvent also called a chiral derivatizing agent (CDA). The first CDA was (α-methoxy-α-(trifluoromethyl)phenylacetic acid) (MTPA also known as Mosher's acid) (Figure 3.130).
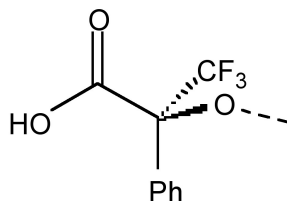
Figure 3.130: The structure of the S-isomer of Mosher's Acid (S-MTPA)

Now, many CDAs exist and are readily available. It should also be noted that CDA development is a current area of active research. In simple terms, one can think of the CDA turning an enantiomeric mixture into a mixture of diastereomeric complexes, producing doublets where each half of the doublet corresponds to each diastereomer, which we already know how to analyze. The resultant peak splitting in the NMR spectra due to diastereomeric interaction can easily determine optical purity. In order to do this, one may simply integrate the peaks corresponding to the different enantiomers thus yielding optical purity of incompletely resolved racemates. One thing of note when performing this experiment is that this interaction between the enantiomeric compounds and the solvent, and thus the magnitude of the splitting, depends upon the asymmetry or chirality of the solvent, the intermolecular interaction between the compound and the solvent, and thus the temperature. Thus, it is helpful to compare the spectra of the enantiomer-CDA mixture with that of the pure enantiomer so that changes in chemical shift can be easily noted.

3.7.5.4 Bibliography

- H. G$\ddot{u}$nther, *NMR Spectroscopy: Basic Principles, Concepts, and Applications in Chemistry*, John Wiley & Sons, Chichester (1996).
- F. A. Bovey, *Nuclear Magnetic Resonance Spectroscopy*, 2nd Ed, Academic, New York (1988).
- S. Braun, H.-O. Kalinowski, S. Berger, *100 and More Basic NMR Experiments: A Practical Course*, VCH, Weinheim (1996).
- A. E. Derome, *Modern NMR Techniques for Chemistry Research* , Pergamon, Oxford (1987).
- J. A. Dale and H. S. Mosher, *J. Am. Chem. Soc.*, 1973, **95**, 512.

3.7.6 Basics of Solid-State NMR[24]

3.7.6.1 Introduction

NMR stands for nuclear magnetic resonance and functions as a powerful tool for chemical characterization. Even though NMR is used mainly for liquids and solutions, technology has progressed to where NMR of solids can be obtained with ease. Aptly named as solid state NMR, the expansion of usable phases has invariably increased our ability to identify chemical compounds. The reason behind difficulties using the solid state lie in the fact that solids are never uniform. When put through a standard NMR, line broadening interactions cannot be removed by rapid molecular motions, which results in unwieldy wide lines which provide little to no useful information. The difference is so staggering that lines broaden by hundreds to thousands of hertz as opposed to less than 0.1 Hz in solution when using an I $= {}^1/_2$ spin nucleus.

A process known as magic angle spinning (MAS), where the sample is tilted at a specific angle, is used in order to overcome line broadening interactions and achieve usable peak resolutions. In order to understand

---

[24]This content is available online at <http://cnx.org/content/m43547/1.1/>.

solid state NMR, its history, operating chemical and mathematical principles, and distinctions from gas phase/solution NMR will be explained.

3.7.6.2 History

The first notable contribution to what we know today as NMR was Wolfgang Pauli's (Figure 3.131) prediction of nuclear spin in 1926. In 1932 Otto Stern (Figure 3.132) used molecular beams and detected nuclear magnetic moments.

Figure 3.131: Austrian theoretical physicist Wolfgang Ernst Pauli (1900-1958).

Figure 3.132: German physicist Otto Stern (1888 - 1969).

Four years later, Gorter performed the first NMR experiment with lithium fluoride (LiF) and hydrated potassium alum ($K[Al(SO_4)_2] \bullet 12H_2O$) at low temperatures. Unfortunately, he was unable to characterize the molecules and the first successful NMR for a solution of water was taken in 1945 by Felix Bloch (Figure 3.133). In the same year, Edward Mills Purcell (Figure 3.134) managed the first successful NMR for the solid paraffin. Continuing their research, Bloch obtained the ^1H NMR of ethanol and Purcell obtained that of paraffin in 1949. In the same year, the chemical significance of chemical shifts was discovered. Finally, high resolution solid state NMR was made possible in 1958 by the discovery of magic angle spinning.
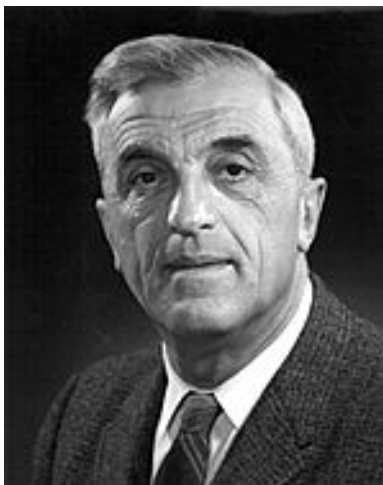
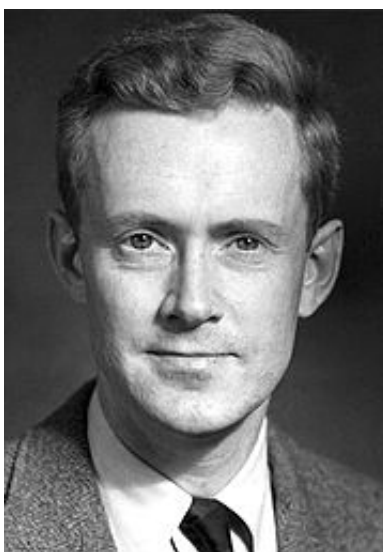**Figure 3.133:** Swiss physicist Felix Bloch (1905-1983).

Figure 3.134: American physicist Edward Mills Purcell (1912-1997).

3.7.6.3 How it works: from machine to graph

NMR spectroscopy works by measuring the nuclear shielding, which can also be seen as the electron density, of a particular element. Nuclear shielding is affected by the chemical environment, as different neighboring

atoms will have different effects on nuclear shielding, as electronegative atoms will tend to decrease shielding and vice versa. NMR requires the elements analyzed to have a spin state greater than zero. Commonly used elements are ^{1}H, ^{13}C, and ^{29}Si. Once inside the NMR machine, the presence of a magnetic field splits the spin states (Figure 3.135).
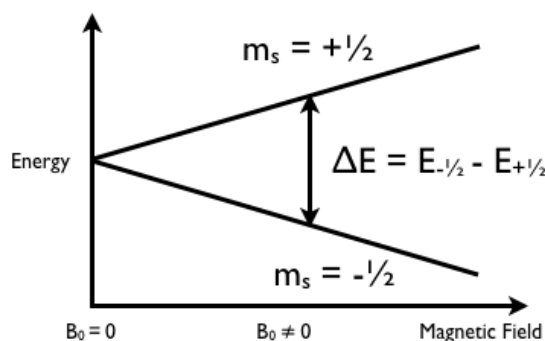

Figure 3.135: Spin state splitting as a function of applied magnetic field.

From (Figure 3.135) we see that a spin state of $^1/_2$ is split into two spin states. As spin state value increases, so does the number of spin states. A spin of 1 will have three spin states, $^3/_2$ will have four spin states, and so on. However, higher spin states increases the difficulty to accurately read NMR results due to confounding peaks and decreased resolution, so spin states of $\frac{1}{2}$ are generally preferred. The E, or radiofrequency shown in (Figure 3.135) can be described by (3.15), where μ is the magnetic moment, a property intrinsic to each particular element. This constant can be derived from (3.16), where Υ is the gyromagnetic ratio, another element dependent quantity, h is Planck's constant, and I is the spin.

$$E = \mu B_0 H_0$$

(3.15)

$$\mu = \gamma h(I(I+1))^{1/2}$$

(3.16)

(3.15) can have E substituted for hν, leading to (3.17), which can solve for the NMR resonance frequency (v).

$$h\nu = \mu B_0 H_0$$

(3.17)

Using the frequency (v), the δ, or expected chemical shift may be computed using (3.18).

$$\delta = \frac{(\nu_{observed} - \nu_{reference})}{\nu_{spectrometer}}$$

(3.18)

Delta (δ) is observed in ppm and gives the distance from a set reference. Delta is directly related to the chemical environment of the particular atom. For a low field, or high delta, an atom is in an environment which produces induces less shielding than in a high field, or low delta.

3.7.6.4 NMR instrument

An NMR can be divided into three main components: the workstation computer where one operates the NMR instrument, the NMR spectrometer console, and the NMR magnet. A standard sample is inserted through the bore tube and pneumatically lowered into the magnet and NMR probe (Figure 3.136).
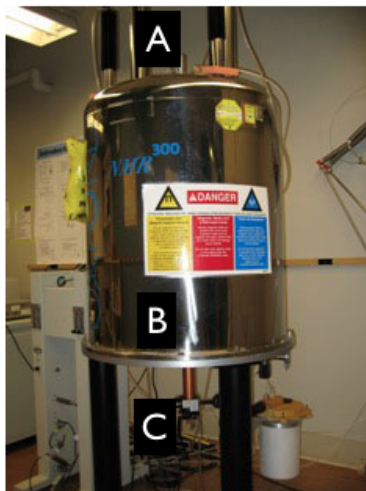

Figure 3.136: Standard NMR instrument, with main components labeled: (A) bore tube, (B) outer magnet shell, (C) NMR probe.

The first layer inside the NMR (Figure 3.137) is the liquid nitrogen jacket. Normally, this space is filled with liquid nitrogen at 77 K. The liquid nitrogen reservoir space is mostly above the magnet so that it can act as a less expensive refrigerant to block infrared radiation from reaching the liquid helium jacket.
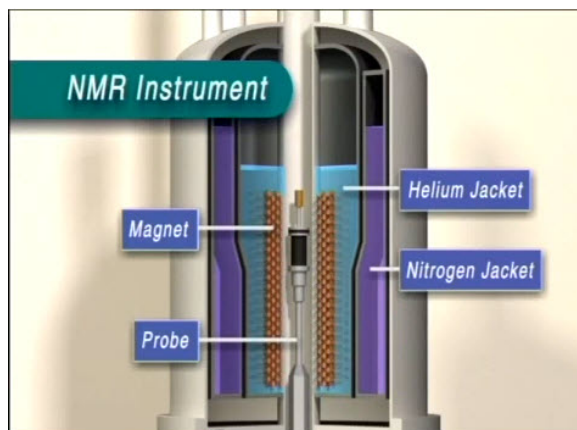
Figure 3.137: Diagram of the main layers inside an NMR machine.

The layer following the liquid nitrogen jacket is a 20 K radiation shield made of aluminum wrapped with alternating layers of aluminum foil and open weave gauze. Its purpose is to block infrared radiation which the 77 K liquid nitrogen vessel was unable to eliminate, which increases the ability for liquid helium to remain in the liquid phase due to its very low boiling point. The liquid helium vessel itself, the next layer, is made of stainless steel wrapped in a single layer of aluminum foil, acting once again as an infrared radiation shield. It is about 1.6 mm thick and kept at 4.2 K.

Inside the vessel and around the magnet is the aluminum baffle, which acts as another degree of infrared radiation protection as well as a layer of protection for the superconducting magnet from liquid helium reservoir fluctuations, especially during liquid helium refills. The significance is that superconducting magnets at low fields are not fully submerged in liquid helium, but higher field superconducting magnets must maintain the superconducting solenoid fully immersed in liquid helium The vapor above the liquid itself is actually enough to maintain superconductivity of most magnets, but if it reaches a temperature above 10 K, the magnet quenches. During a quench, the solenoid exceeds its critical temperature for superconductivity and becomes resistive, generating heat. This heat, in turn, boils off the liquid helium. Therefore, a small opening at the very base of the baffle exists as a path for the liquid helium to reach the magnet surface so that during refills the magnet is protected from accidental quenching.

3.7.6.5 Problems with solid state NMR

The most notable difference between solid samples and solution/gas in terms of NMR spectroscopy is that molecules in solution rotate rapidly while those in a solid are fixed in a lattice. Different peak readings will be produced depending on how the molecules are oriented in the magnetic field because chemical shielding depends upon the orientation of a molecule, causing chemical shift anisotropy. Therefore, the effect of chemical shielding also depends upon the orientation of the molecule with respect to the spectrometer. These counteracting forces are balanced out in gases and solutions because of their randomized molecular movement, but become a serious issue with fixed molecules observed in solid samples. If the chemical shielding isn't determined accurately, neither will the chemical shifts (δ).

Another issue with solid samples are dipolar interactions which can be very large in solid samples causing linewidths of tens to hundreds of kilohertz to be generated. Dipolar interactions are tensor quantities, which demonstrate values dependent on the orientation and placement of a molecule in reference to its surroundings. Once again the issue goes back to the lattice structure of solids, which are in a fixed location.

Even though the molecules are fixed, this does not mean that nuclei are evenly spread apart. Closer nuclei display greater dipolar interactions and vice versa, creating the noise seen in spectra of NMR not adapted for solid samples. Dipolar interactions are averaged out in solution states because of randomized movement. Spin state repulsions are averaged out by molecular motion of solutions and gases. However, in solid state, these interactions are not averaged and become a third source of line broadening.

3.7.6.5.1 Magic angle spinning

In order to counteract chemical shift anisotropy and dipolar interactions, magic angle spinning was developed. As discussed above, describing dipolar splitting and chemical shift aniostoropy interactions respectively, it becomes evident that both depend on the geometric factor $(3\cos^2\theta\text{-}1)$.

$$\text{Dipolar splitting } = \text{ } C(\mu_0/8\pi)(\gamma_a\gamma_x/r^2_{ax})(3\cos^2\theta_{iz}\text{-}1)$$

(3.19)

$$\sigma_{zz} = \overline{\sigma} + {}^1\!/_3\Sigma\sigma_{ii}(3\cos^2\theta_{iz}\text{-}1)$$

(3.20)

If this factor is decreased to 0, then line broadening due to chemical shift anisotropy and dipolar interactions will disappear. Therefore, solid samples are rotated at an angle of $54.74\,^\circ$, effectively allowing solid samples to behave similarly to solutions/gases in NMR spectroscopy. Standard spinning rates range from 12 kHz to an upper limit of 35 kHz, where higher spin rates are necessary to remove higher intermolecular interactions.

3.7.6.6 Application of solid state NMR

The development of solid state NMR is a technique necessary to understand and classify compounds that would not work well in solutions, such as powders and complex proteins, or study crystals too small for a different characterization method.

Solid state NMR gives information about local environment of silicon, aluminum, phosphorus, etc. in the structures, and is therefore an important tool in determining structure of molecular sieves. The main issue frequently encountered is that crystals large enough for X-Ray crystallography cannot be grown, so NMR is used since it determines the local environments of these elements. Additionally, by using ^{13}C and ^{15}N, solid state NMR helps study amyloid fibrils, filamentous insoluble protein aggregates related to neurodegenerative diseases such as Alzheimer's disease, type II diabetes, Huntington's disease, and prion diseases.

3.7.6.7 Bibliography

- J. W. Akitt, *NMR and Chemistry*, 3$^\text{rd}$ Edn., Chapman & Hall, London (1992).
- A. R. Grimmer and B. Blümich, *Introduction to Solid-State NMR*, Springer-Verlag, Berlin(1994).
- J. A. Iggo, *NMR Spectroscopy in Inorganic Chemistry*, Oxford University Press, New York (1999).
- J. C. C. Chan, *Top. Curr. Chem.*, 2011, **306**, 47.
- R. Freeman, *Chem Heterocyc Compd*, 1995, **31**, 1004-1005.
- Jeol USA, *JEOL Delta-GSX 270 NMR Magnet Destruction*, <http://www.jeolusa.com>
- University of Pittsburgh, *Magnet Safety*, <http://www.ehs.pitt.edu/assets/docs/magnet-safety.pdf>, 2008, (accessed 15 February 2012).

3.7.7 Using 13-C NMR to Study Carbon Nanomaterials[25]

3.7.7.1 Introduction

3.7.7.1.1 Carbon nanomaterial

There are several types of carbon nanomaterial. Members of this family are graphene, single-walled carbon nanotubes (SWNT), multi-walled carbon nanotubes (MWNT), and fullerenes such as C_{60}. Nano materials have been subject to various modification and functionalizations, and it has been of interest to develop methods that could observe these changes. Herein we discuss selected applications of ^{13}C NMR in studying graphene and SWNTs. In addition, a discussion of how ^{13}C NMR could be used to analyze a thin film of amorphous carbon during a low-temperature annealing process will be presented.

3.7.7.1.2 ^{13}C NMR versus ^1H NMR

Since carbon is found in any organic molecule NMR that can analyze carbon could be very helpful, unfortunately the major isotope, ^{12}C, is not NMR active. Fortunately, ^{13}C with a natural abundance of 1.1% is NMR active. This low natural abundance along with lower gyromagnetic ratio for ^{13}C causes sensitivity to decrease. Due to this lower sensitivity, obtaining a ^{13}C NMR spectrum with a specific signal-to-noise ratio requires averaging more spectra than the number of spectra that would be required to average in order to get the same signal to noise ratio for a ^1H NMR spectrum. Although it has a lower sensitivity, it is still highly used as it discloses valuable information.

Peaks in a ^1H NMR spectrum are split to *n + 1* peak, where *n* is the number of hydrogen atoms on the adjacent carbon atom. The splitting pattern in ^{13}C NMR is different. First of all, C-C splitting is not observed, because the probability of having two adjacent ^{13}C is about 0.01%. Observed splitting patterns, which is due to the hydrogen atoms on the same carbon atom not on the adjacent carbon atom, is governed by the same *n + 1* rule.

In ^1H NMR, the integral of the peaks are used for quantitative analysis, whereas this is problematic in ^{13}C NMR. The long relaxation process for carbon atoms takes longer comparing to that of hydrogen atoms, which also depends on the order of carbon (i.e., 1°, 2°, etc.). This causes the peak heights to not be related to the quantity of the corresponding carbon atoms.

Another difference between ^{13}C NMR and ^1H NMR is the chemical shift range. The range of the chemical shifts in a typical NMR represents the different between the minimum and maximum amount of electron density around that specific nucleus. Since hydrogen is surrounded by fewer electrons in comparison to carbon, the maximum change in the electron density for hydrogen is less than that for carbon. Thus, the range of chemical shift in ^1H NMR is narrower than that of ^{13}C NMR.

3.7.7.1.3 Solid state NMR

^{13}C NMR spectra could also be recorded for solid samples. The peaks for solid samples are very broad because the sample, being solid, cannot have all anisotropic, or orientation-dependent, interactions canceled due to *rapid random tumbling*. However, it is still possible to do high resolution solid state NMR by spinning the sample at 54.74° with respect to the applied magnetic field, which is called the *magic angle*. In other words, the sample can be spun to artificially cancel the orientation-dependent interaction. In general, the spinning frequency has a considerable effect on the spectrum.

3.7.7.2 ^{13}C NMR of carbon nanotubes

Single-walled carbon nanotubes contain sp^2 carbons. Derivatives of SWNTs contain sp^3 carbons in addition. There are several factors that affect the ^{13}C NMR spectrum of a SWNT sample, three of which will be reviewed in this module: ^{13}C percentage, diameter of the nanotube, and functionalization.

---

[25]This content is available online at <http://cnx.org/content/m46153/1.2/>.

3.7.7.2.1 ^{13}C percentage

For sp^2 carbons, there is a slight dependence of ^{13}C NMR peaks on the percentage of ^{13}C in the sample. Samples with lower ^{13}C percentage are slighted shifted downfield (higher ppm). Data are shown in Table 3.21. Please note that these peaks are for the sp^2 carbons.

Sample	δ (ppm)
SWNTs(100%)	116±1
SWNTs(1%)	118±1

Table 3.21: Effects of ^{13}C percentage on the sp^2 peak. Data from S. Hayashi, F. Hoshi, T. Ishikura, M. Yumura, and S. Ohshima, *Carbon*, 2003, **41**, 3047.

3.7.7.2.2 Diameter of the nanotubes

The peak position for SWNTs also depends on the diameter of the nanotubes. It has been reported that the chemical shift for sp^2 carbons decreases as the diameter of the nanotubes increases. Figure 3.138 shows this correlation. Since the peak position depends on the diameter of nanotubes, the peak broadening can be related to the diameter distribution. In other words, the narrower the peak is, the smaller the diameter distribution of SWNTs is. This correlation is shown in Figure 3.139.
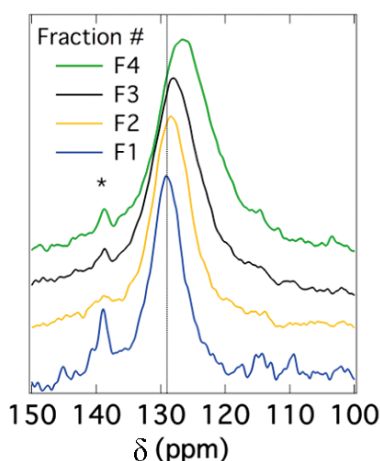

Figure 3.138: Correlation between the chemical shift of the sp^2 carbon and the diameter of the nanotubes. The diameter of the nanotubes increases from F1 to F4. Image from C. Engtrakul, V. M. Irurzun, E. L. Gjersing, J. M. Holt, B. A. Larsen, D. E. Resasco, and J. L. Blackburn, *J. Am. Chem. Soc.*, 2012, **134**, 4850. Copyright: American Chemical Society (2012).
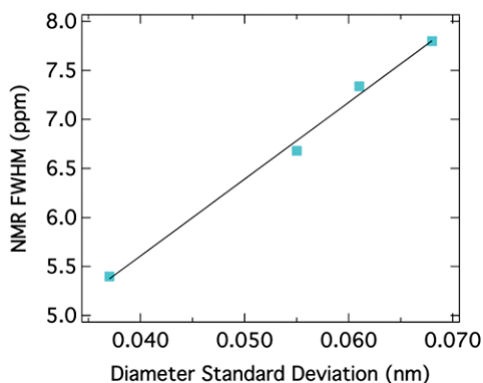
Figure 3.139: Correlation between FWHM and the standard deviation of the diameter of nanotubes. Image from C. Engtrakul, V. M. Irurzun, E. L. Gjersing, J. M. Holt, B. A. Larsen, D. E. Resasco, and J. L. Blackburn, *J. Am. Chem. Soc.*, 2012, **134**, 4850. Copyright: American Chemical Society (2012).

3.7.7.2.3 Functionalization

Solid stated ^{13}C NMR can also be used to analyze functionalized nanotubes. As a result of functionalizing SWNTs with groups containing a carbonyl group, a slight shift toward higher fields (lower ppm) for the sp^2 carbons is observed. This shift is explained by the perturbation applied to the electronic structure of the whole nanotube as a result of the modifications on only a fraction of the nanotube. At the same time, a new peak emerges at around 172 ppm, which is assigned to the carboxyl group of the substituent. The peak intensities could also be used to quantify the level of functionalization. Figure 3.140 shows these changes, in which the substituents are $-(CH_2)_3COOH$, $-(CH_2)_2COOH$, and $-(CH_2)_2CONH(CH_2)_2NH_2$ for the spectra Figure 3.140b, Figure 3.140c, and Figure 3.140d, respectively. Note that the bond between the nanotube and the substituent is a C-C bond. Due to low sensitivity, the peak for the sp^3 carbons of the nanotube, which does not have a high quantity, is not detected. There is a small peak around 35 ppm in Figure 3.140, can be assigned to the aliphatic carbons of the substituent.
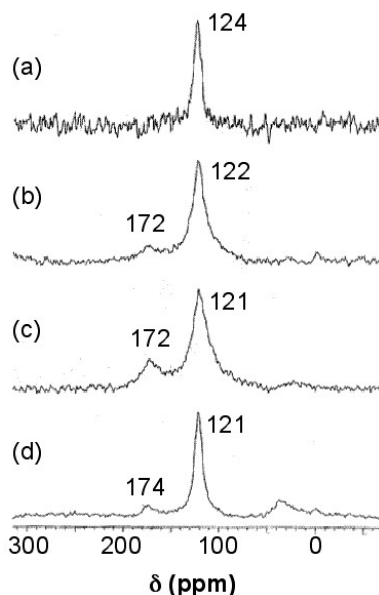
Figure 3.140: ^{13}C NMR spectra for (a) pristine SWNT, (b) SWNT functionalized with –$(CH_2)_3COOH$, (c) SWNT functionalized with –$(CH_2)_2COOH$, and (d) SWNT functionalized with –$(CH_2)_2CONH(CH_2)_2NH_2$. Image from H. Peng, L. B. Alemany, J. L. Margrave, and V. N. Khabashesku, *J. Am. Chem. Soc.*, 2003, **125**, 15174. Copyright: American Chemical Society (2003).

For substituents containing aliphatic carbons, a new peak around 35 ppm emerges, as was shown in Figure 3.140, which is due to the aliphatic carbons. Since the quantity for the substituent carbons is low, the peak cannot be detected. Small substituents on the sidewall of SWNTs can be chemically modified to contain more carbons, so the signal due to those carbons could be detected. This idea, as a strategy for enhancing the signal from the substituents, can be used to analyze certain types of sidewall modifications. For example, when Gly (–$NH_2CH_2CO_2H$) was added to F-SWNTs (fluorinated SWNTs) to substitute the fluorine atoms, the ^{13}C NMR spectrum for the Gly-SWNTs was showing one peak for the sp^2 carbons. When the aliphatic substituent was changed to 6-aminohexanoic acid with five aliphatic carbons, the peak was detectable, and using 11-aminoundecanoic acid (ten aliphatic carbons) the peak intensity was in the order of the size of the peak for sp^2 carbons. In order to use ^{13}C NMR to enhance the substituent peak (for modification quantification purposes as an example), Gly-SWNTs was treated with 1-dodecanol to modify Gly to an amino ester. This modification resulted in enhancing the aliphatic carbon peak at around 30 ppm. Similar to the results in Figure 3.140, a peak at around 170 emerged which was assigned to the carbonyl carbon. The sp^3 carbon of the SWNTs, which was attached to nitrogen, produced a small peak at around 80 ppm, which is detected in a cross-polarization magic angle spinning (CP-MAS) experiment.

F-SWNTs (fluorinated SWNTs) are reported to have a peak at around 90 ppm for the sp^3 carbon of nanotube that is attached to the fluorine. The results of this part are summarized in Table 3.22 (approximate values).

Group	δ (ppm)	Intensity
sp^2 carbons of SWNTs	120	Strong
$-NH_2(CH_2)_n CO_2H$ (aliphatic carbon, n=1,5, 10)	20-40	Depends on 'n'
$-NH_2(CH_2)_n CO_2H$ (carboxyl carbon, n=1,5, 10)	170	Weak
sp^3 carbon attached to nitrogen	80	Weak
sp^3 carbon attached to fluorine	90	Weak

Table 3.22: Chemical shift for different types of carbons in modified SWNTs. Note that the peak for the aliphatic carbons gets stronger if the amino acid is esterified. Data are obtained from: H. Peng, L. B. Alemany, J. L. Margrave, and V. N. Khabashesku, *J. Am. Chem. Soc.*, 2003, **125**, 15174; L. Zeng, L. Alemany, C. Edwards, and A. Barron, *Nano. Res.*, 2008, **1**, 72; L. B. Alemany, L. Zhang, L. Zeng, C. L. Edwards, and A. R. Barron, *Chem. Mater.*, 2007, **19**, 735.

The peak intensities that are weak in Table 3.22 depend on the level of functionalization and for highly functionalized SWNTs, those peaks are not weak. The peak intensity for aliphatic carbons can be enhanced as the substituents get modified by attaching to other molecules with aliphatic carbons. Thus, the peak intensities can be used to quantify the level of functionalization.

3.7.7.3 ^{13}C NMR of functionalized graphene

Graphene is a single layer of sp^2 carbons, which exhibits a benzene-like structure. Functionalization of graphene sheets results in converting some of the sp^2 carbons to sp^3. The peak for the sp^2 carbons of graphene shows a peak at around 140 ppm. It has been reported that fluorinated graphene produces an sp^3 peak at around 82 ppm. It has also been reported for graphite oxide (GO), which contains $-OH$ and epoxy substituents, to have peaks at around 60 and 70 ppm for the epoxy and the $-OH$ substituents, respectively. There are chances for similar peaks to appear for graphene oxide. Table 3.23 summarizes these results.

Type of carbon	δ (ppm)
sp^2	140
sp^3 attached to fluorine	80
sp^3 attached to $-OH$ (for GO)	70
sp^3 attached to epoxide (for GO)	60

Table 3.23: Chemical shifts for functionalized graphene. Data are obtained from: M. Dubois, K. Guérin, J. P. Pinheiro, Z. Fawal, F. Masin, and A. Hamwi, *Carbon*, 2004, **42**, 1931; L. B. Casabianca, M. A. Shaibat, W. W. Cai, S. Park, R. Piner, R. S. Ruoff, and Y. Ishii, *J. Am. Chem. Soc.*, 2010, **132**, 5672.

3.7.7.4 Analyzing annealing process using ^{13}C NMR

^{13}C NMR spectroscopy has been used to study the effects of low-temperature annealing (at 650 °C) on thin films of amorphous carbon. The thin films were synthesized from a ^{13}C enriched carbon source (99%). There were two peaks in the ^{13}C NMR spectrum at about 69 and 142 ppm which were assigned to sp^3 and sp^2 carbons, respectively (Figure 3.141). The intensity of each peak was used to find the percentage of each type of hybridization in the whole sample, and the broadening of the peaks was used to estimate the distribution of different types of carbons in the sample. It was found that while the composition of the sample didn't change during the annealing process (peak intensities didn't change, see Figure 3.141b), the full width at half maximum (FWHM) did change (Figure 3.141a). The latter suggested that the structure became more

ordered, i.e., the distribution of sp^2 and sp^3 carbons within the sample became more homogeneous. Thus, it was concluded that the sample turned into a more homogenous one in terms of the distribution of carbons with different hybridization, while the fraction of sp^2 and sp^3 carbons remained unchanged.
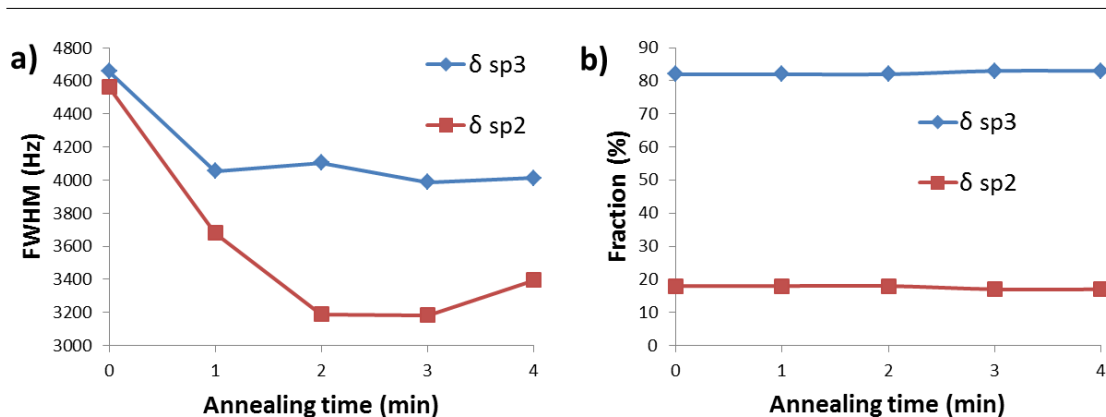

Figure 3.141: a) Effect of the annealing process on the FWHM, which represents the change in the distribution of sp^2 and sp^3 carbons. b) Fractions of sp^2 and sp^3 carbon during the annealing process. Data are obtained from T. M. Alam, T. A. Friedmann, P. A. Schultz, and D. Sebastiani, *Phys. Rev. B.*, 2003, **67**, 245309.

Aside from the reported results from the paper, it can be concluded that ^{13}C NMR is a good technique to study annealing, and possibly other similar processes, in real time, if the kinetics of the process is slow enough. For these purposes, the peak intensity and FWHM can be used to find or estimate the fraction and distribution of each type of carbon respectively.

3.7.7.5 Summary

^{13}C NMR can reveal important information about the structure of SWNTs and graphene. ^{13}C NMR chemical shifts and FWHM can be used to estimate the diameter size and diameter distribution. Though there are some limitations, it can be used to contain some information about the substituent type, as well as be used to quantify the level of functionalization. Modifications on the substituent can result in enhancing the substituent signal. Similar type of information can be achieved for graphene. It can also be employed to track changes during annealing and possibly during other modifications with similar time scales. Due to low natural abundance of ^{13}C it might be necessary to synthesize ^{13}C-enhanced samples in order to obtain suitable spectra with a sufficient signal-to-noise ratio. Similar principles could be used to follow the annealing process of carbon nano materials. C$_{60}$ will not be discussed herein.

3.7.7.6 Bibliography

- T. M. Alam, T. A. Friedmann, P. A. Schultz, and D. Sebastiani, *Phys. Rev. B.*, 2003, **67**, 245309.
- L. B. Alemany, L. Zhang, L. Zeng, C. L. Edwards, and A. R. Barron, *Chem. Mater.*, 2007, **19**, 735.
- L. B. Casabianca, M. A. Shaibat, W. W. Cai, S. Park, R. Piner, R. S. Ruoff, and Y. Ishii, *J. Am. Chem. Soc.*, 2010, **132**, 5672.
- M. Dubois, K. Guérin, J. P. Pinheiro, Z. Fawal, F. Masin, and A. Hamwi, *Carbon*, 2004, **42**, 1931.

- C. Engtrakul, V. M. Irurzun, E. L. Gjersing, J. M. Holt, B. A. Larsen, D. E. Resasco, and J. L. Blackburn, *J. Am. Chem. Soc.*, 2012, **134**, 4850.
- S. Hayashi, F. Hoshi, T. Ishikura, M. Yumura, and S. Ohshima, *Carbon*, 2003, **41**, 3047.
- H. Peng, L. B. Alemany, J. L. Margrave, and V. N. Khabashesku, *J. Am. Chem. Soc.*, 2003, **125**, 15174.
- L. Zeng, L. Alemany, C. Edwards, and A. Barron, *Nano. Res.*, 2008, **1**, 72.

3.7.8 Lanthanide Shift Reagents[26]

3.7.8.1 Introduction

Nuclear magnetic resonance spectroscopy (NMR) is the most powerful tool for organic and organometallic compound determination. Even structures can be determined just using this technique. In general NMR gives information about the number of magnetically distinct atoms of the specific nuclei under study, as well as information regarding the nature of the immediate environment surrounding each nuclei. Because hydrogen and carbon are the major components of organic and organometallic compounds, proton (^{1}H) NMR and carbon-13 (^{13}C) NMR are the most useful nuclei to observe.

Not all the protons experience resonance at the same frequency in a ^{1}H NMR, and thus it is possible to differentiate between them. The diversity is due to the existence of a different electronic environment around chemically different nuclei. Under an external magnetic field (B_0), the electrons in the valence shell are affected; they start to circulate generating a magnetic field, which is apposite to the applied magnetic field. This effect is called diamagnetic shielding or diamagnetic anisotropy (Figure 3.142).

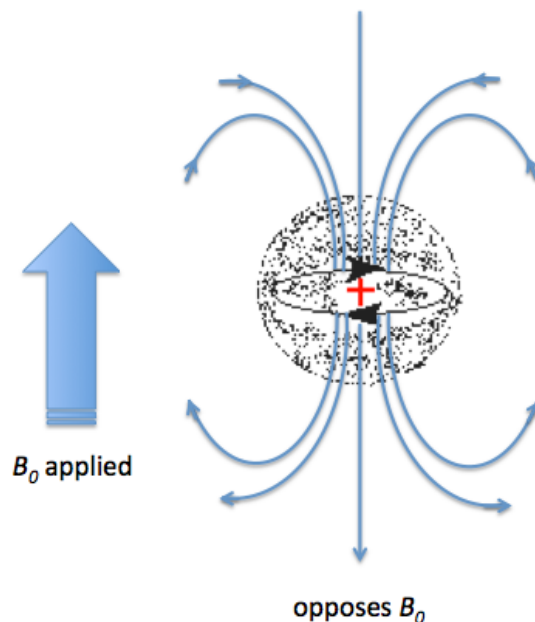[26]This content is available online at <http://cnx.org/content/m43580/1.1/>.

Figure 3.142: Schematic representation of diamagnetic anisotropy. Adapted from D. L. Pavia, G. M. Lampman, and G. S. Kriz, *Introduction to Spectroscopy*, 3th Ed., Thomson Learning, Tampa, FL, (2011).

The greater the electron density around one specific nucleus, the greater will be the induced field that opposes the applied field, and this will result in a different resonance frequency. The identification of protons sounds simple, however, the NMR technique has a relatively low sensitivity of proton chemical shifts to changes in the chemical and stereochemical environment; as a consequence the resonance of chemically similar proton overlap. There are several methods that have been used to resolve this problem, such as: the use of higher frequency spectrometers or by the use of shift reagents as aromatic solvents or lanthanide complexes. The main issue with high frequency spectrometers is that they are very expensive, which reduces the number of institutions that can have access to them. In contrast, shift reagents work by reducing the equivalence of nuclei by altering their magnetic environment, and can be used on any NMR instrument. The simplest shift reagent is the one of different solvents, however problems with some solvents is that they can react with the compound under study, and also that these solvents usually just alter the magnetic environment of a small part of the molecule. Consequently, although there are several methods, most of the work has been done with lanthanide complexes.

3.7.8.2 The history of lanthanide shift reagents

The first significant induced chemical shift using paramagnetic ions was reported in 1969 by Conrad Hinckley (Figure 3.143), where he used bispyridine adduct of tris(2,2,6,6-tetramethylhepta-3,5-dionato)europium(III) (Eu(tmhd)$_3$), better known as Eu(dpm)$_3$, where dpm is the abbreviation of dipivaloyl- methanato, the chemical structure is shown in Figure 3.144. Hinckley used Eu(tmhd)$_3$ on the ^{1}H NMR spectrum of cholesterol from $347 - 2$ Hz. The development of this new chemical method to improve the resolution of the NMR spectrum was the stepping-stone for the work of Jeremy Sanders and Dudley Williams, Figure 3.145 and Figure 3.146 respectively. They observed a significant increase in the magnitude of the induced shift after

using just the lanthanide chelate without the pyridine complex. Sugesting that the pyridine donor ligands are in competition for the active sides of the lanthanide complex. The efficiency of Eu(tmhd)$_3$ as a shift reagent was published by Sanders and Williams in 1970, where they showed a significant difference in the ^{1}H NMR spectrum of n-pentanol using the shift reagent, see Figure 3.147.

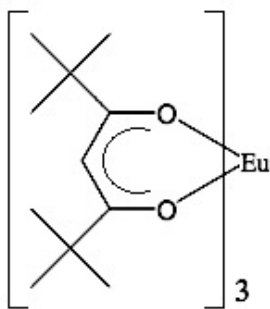**Figure 3.143:** Chemist Conrad Hinclley, Emeritus professor in Southern Illinois University..

Figure 3.144: Chemical structure of Eu(tmhd)$_3$.

Figure 3.145: British chemist Jeremy Keith Morris Sanders.

Figure 3.146: British chemist Dudley Williams (1937-2010).
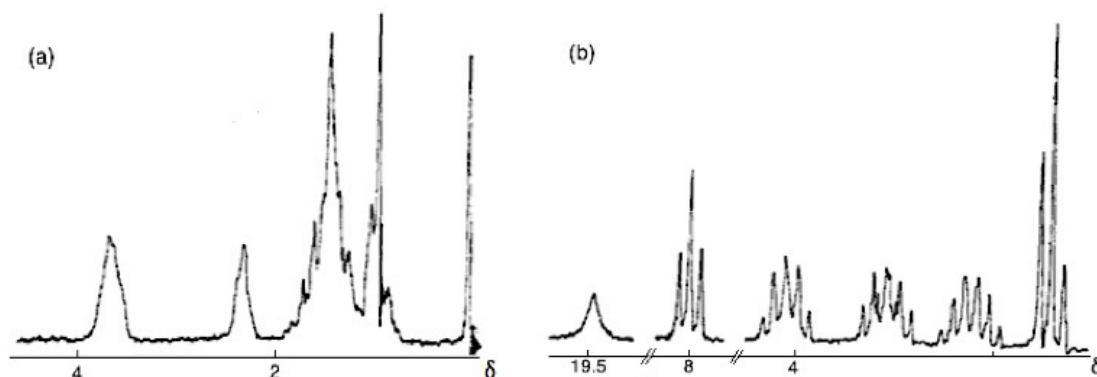
Figure 3.147: ^{1}H NMR spectra of n-pentanol, (a) without the present of lanthanide reagents and (b) in the present of the lanthanide reagent Eu(tmhd)$_3$. Adapted from *Chem Reviews*, 1973, **73**, 553. Copyright: American Chemical Society 1973.

Analyzing the spectra in Figure 3.147 it is easy to see that with the use of Eu(tmhd)$_3$ there is any overlap between peaks. Instead, the multiplets of each proton are perfectly clear. After these two publications the potential of lanthanide as shift reagents for NMR studies became a popular topic. Other example is the fluorinate version of Eu(dpm)$_3$; (*tris*(7,7,-dimethyl-1,1,2,2,2,3,3-heptafluoroocta-7,7-dimethyl-4,6-dionato)europium(III), best known as Eu(fod)$_3$, which was synthesized in 1971 by Rondeau and Sievers. This LSR presents better solubility and greater Lewis acid character, the chemical structure is show in Figure 3.148.
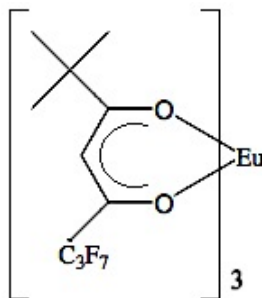

Figure 3.148: Chemical structure of (*tris*(7,7,-dimethyl-1,1,2,2,2,3,3-heptafluoroocta-7,7-dimethyl-4,6-dionato)europium(III).

3.7.8.3 Mechanism of inducement of chemical shift

Lanthanide atoms are Lewis acids, and because of that, they have the ability to cause chemical shift by the interaction with the basic sites in the molecules. Lanthanide metals are especially effective over other metals because there is a significant delocalization of the unpaired f electrons onto the substrate as a consequence of unpaired electrons in the f shell of the lanthanide. The lanthanide metal in the complexes interacts with the relatively basic lone pair of electrons of aldehydes, alcohols, ketones, amines and other functional groups within the molecule that have a relative basic lone pair of electrons, resulting in a NMR spectral simplification.

There are two possible mechanisms by which a shift can occur: shifts by contact and shifts by pseudo-contact. The first one is a result of the transfer of electron spin density via covalent bond formation from the lanthanide metal ion to the associated nuclei. While the magnetic effects of the unpaired electron magnetic moment causes the pseudocontact shift. Lanthanide complexes give shifts primarily by the pseudocontact mechanism. Under this mechanism, there are several factors that influence the shift of a specific NMR peak. The principal factor is the distance between the metal ion and the proton; the shorter the distance, the greater the shift obtained. On the other hand, the direction of the shift depends on the lanthanide complex used. The complexes that produce a shift to a lower field (downfield) are the ones containing erbium, europium, thulium and ytterbium, while complexes with cerium, neodymium, holmium, praseodymium, samarium and terbium, shift resonances to higher field. Figure 6 shows the difference betwen an NMR spectrum without the use of shift reagent versus the same spectrum in the present of a europium complex (downfield shift) and a praseodymium complex (high-field shift).
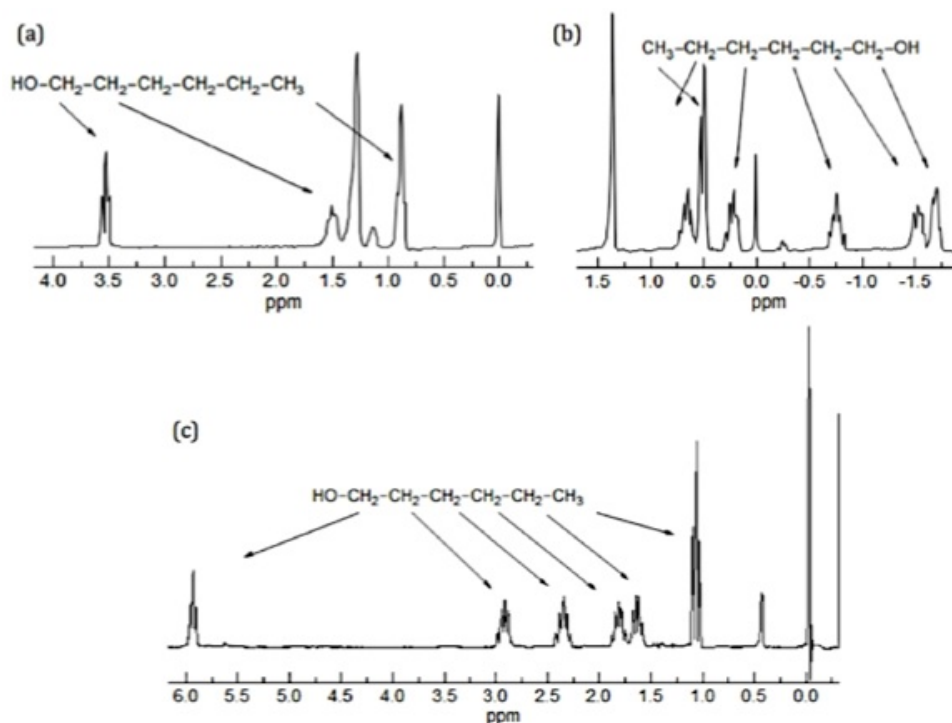
Figure 3.149: (a) ^{1}H NMR spectrum of n-hexanol without the present of shift reagents. (b) ^{1}H NMR spectrum of n-hexanol in present of 14% Pr(fod)$_3$ and the thirt spectrum (c) is the ^{1}H NMR spectrum of n-hexanol in the present of 6.5% Eu(fod)$_3$. Adapted from http://www.chem.wisc.edu/areas/reich/nmr/08-tech-07-lis.htm[27]

Linewidth broadening is not desired because of loss of resolution, and lanthanide complexes unfortunately contribute extremely to this effect when they are used in high concentrations due to their mechanism that shortens the relaxation times (T_2), which in turn increases the bandwidth. However europium and praseodymium are an extraordinary exception giving a very low shift broadening, 0.003 and 0.005 Hz/Hz respectively. Europium specially is the most used lanthanide as shift reagent because of its inefficient nuclear spin-lattice ratio properties. It has low angular momentum quantum numbers and a diamagnetic 7F0 ground state. These two properties contribute to a very small separation of the highest and lowest occupied metal orbitals leading to an inefficient relaxation and a very little broadening in the NMR spectra. The excited 7F1 state will then contribute to the pseudocontact shift.

We have mentioned above that lanthanide complexes have a mechanism that influences relaxation times, and this is certainly because paramagnetic ions have an influence in both: chemical shifts and relaxation rates. The relaxation times are of great significant because they depend on the width of a specific resonance (peak). Changes in relaxation time could also be related with the geometry of the complex.

3.7.8.4 Measuring the shift

The easiest and more practical way to measure the lanthanide-induced shift (LIS) is to add aliquots of the lanthanide shift reagent (LSR or Δvi) to the sample that has the compound of interest (substrate), and take

---

[27]http://www.chem.wisc.edu/areas/reich/nmr/08-tech-07-lis.htm

an NMR spectra after each addition. Because the shift of each proton will change after each addition of the LSR to lower or upper field, the LIS can me measured. With the data collected, a plot of the LIS against the ratio of LSR: substrate will generate a straight line where the slope is representative of the compound that is being studied. The identification of the compound by the use of chiral lanthanide shift reagents can be so precise that it is possible to estimate the composition of enantiomers in the solution under study, see Figure 3.150.
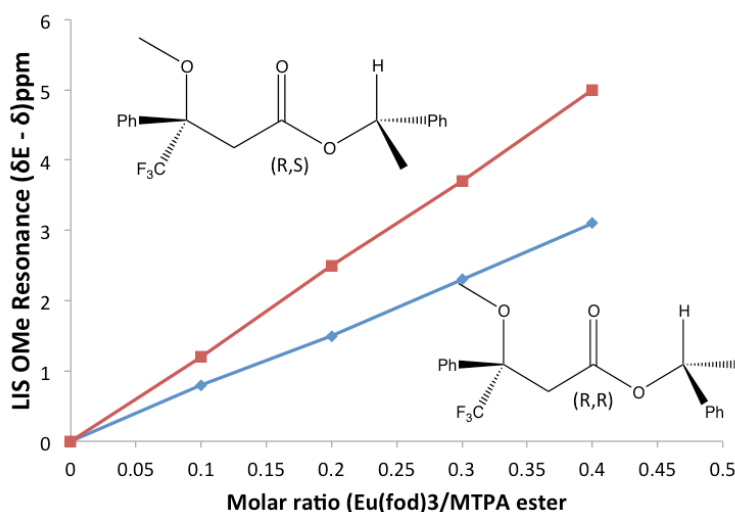
Figure 3.150: Lanthanide induced shift of methoxyl proton resonance versus molar ratio of Eu(fod)$_3$, for the diastereomeric MTPA esters. δ is the normal chemical shift and δ_E is the chemical shift in ppm for the OMe signal in the presence of a specified molar ratio of Eu(fod)$_3$, in CCl$_4$ as solvent. Adapted from S. Yamaguchi, F. Yasuhara and K. Kabuto, *Tetrahedron*, 1976, **32**, 1363.

Now, what is the mechanism that is actually happening between the LSR and the compound under study? The LSR is a metal complex of six coordinate sides. The LSR, in presence of substrate that contains heteroatoms with Lewis basicity character, expands its coordination sides in solution in order to accept additional ligands. An equilibrium mixture is formed between the substrate and the LSR. (3.21) and (3.22) show the equilibrium, where L is LSR, S is the substrate, and LS is the concentration of the complex formed is solution.

$$ L \ + \ S \ \underset{}{\overset{K_1}{\rightleftharpoons}} \ [LS] \tag{3.21}$$

$$ [LS] \ + \ S \ \underset{}{\overset{K_2}{\rightleftharpoons}} \ [LS_2] \tag{3.22}$$
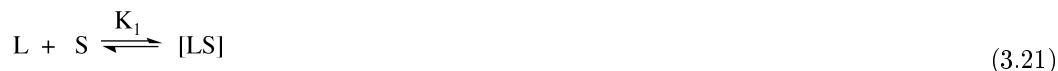
The abundance of these species depends on K_1 and K_2, which are the binding constant. The binding constant is a special case of equilibrium constant, but it refers with the binding and unbinding mechanism of two species. In most of the cases like, K_2 is assumed to be negligible and therefore just the first complex [LS] is assumed to be formed. The equilibrium between L + S and LS in solution is faster than the NMR timescale, consequently a single average signal will be recorded for each nucleus.

3.7.8.5 Determination of enantiomeric purity

Besides the great potential of lanthanide shift reagents to improve the resolution of NMR spectrums, these complexes also have been used to identify enantiomeric mixtures in solution. To make this possible the substrate must meet certain properties. The fist one is that the organic compounds in the enantiomeric composition must to have a hard organic base as functional group. The shift reagents are not effective with most of the soft bases. Though hundreds of chelates have been synthesized after $Eu(dcm)_3$, this one is the LSR that resulted in the most effective reagent for the resolution of enantiotopic resonances. Basically if you take an NMR of an enantiomeric mixture sample, a big variety of peaks will appear and the hard part is to identify which of those peaks correspond to which specific enantiomer. The differences in chemical shifts observed for enantiomeric mixtures in solution containing LSR might arise from at least two sources: the equilibrium constants of the formation of the possible diastereometic complexes between the substrate and the LSR, and the geometries of these complexes, which might be distinct. The enantiomeric shift differences sometimes are defined as $\Delta\Delta\delta$.

In solution the exchange between substrate coordinated to the europium ion and the free substrate in solution is very fast. To be sure that the europium complexes are binding with one or two substrate molecules, an excess of substrate is usually added.

3.7.8.6 Biography

- L. G. Wade, Jr., *Organic Chemistry*, 4th edn., Upper Saddle River, New Jersey (2006).
- D. L. Pavia, G. M. Lampman, and G. S. Kriz, *Introduction to Spectroscopy*, 3th edn., Bellinghan, WA (2001).
- J. B. Lambert and E. P. Mazzola, *Nuclear Magnetic Resonance Spectroscopy*, Upper Saddle River, New Jersey (2004).
- C. C. Hinckley, *J. Am. Chem. Soc.*, 1969, **91**, 5160.
- J. K. M. Sanders and D. H. Williams, *J. Am. Chem. Soc.*, 971, **93**, 1641.
- A. F. Cockerill, G. L. O. Davies, R. C. Harden, and D. M. Rackham, *Chem. Rev.*, 1973, **73**, 553.
- B. C. Mayor, *J. Am. Chem. Soc.*, 1969, **91**, 49.
- S. Yamaguchi, F. Yasuhara, and K. Kabuto, *Tetrahedron*, 1976, **32**, 1363.

3.8 EPR Spectroscopy

3.8.1 EPR Spectroscopy: An Overview[28]

3.8.1.1 Basic principles for EPR spectroscopy

Electron paramagnetic resonance spectroscopy (EPR) is a powerful tool for investigating paramagnetic species, including organic radicals, inorganic radicals, and triplet states. The basic principles behind EPR are very similar to the more ubiquitous nuclear magnetic resonance spectroscopy (NMR), except that EPR focuses on the interaction of an external magnetic field with the unpaired electron(s) in a molecule, rather than the nuclei of individual atoms. EPR has been used to investigate kinetics, mechanisms, and structures of paramagnetic species and along with general chemistry and physics, has applications in biochemistry, polymer science, and geosciences.

The degeneracy of the electron spin states is lifted when an unpaired electron is placed in a magnetic field, creating two spin states, $m_s = \pm \frac{1}{2}$, where $m_s = -\frac{1}{2}$, the lower energy state, is aligned with the magnetic field. The spin state on the electron can flip when electromagnetic radiation is applied. In the case of electron spin transitions, this corresponds to radiation in the microwave range.

The energy difference between the two spin states is given by the equation

$\Delta E = E_+ - E_- = h\nu = g\beta B$

---

[28]This content is available online at <http://cnx.org/content/m22370/1.3/>.

where h is Planck's constant (6.626×10^{-34} J s^{-1}), v is the frequency of radiation, ß is the Bohr magneton (9.274×10^{-24} J T^{-1}), B is the strength of the magnetic field in Tesla, and g is known as the g-factor. The g-factor is a unitless measurement of the intrinsic magnetic moment of the electron, and its value for a free electron is 2.0023. The value of g can vary, however, and can be calculated by rearrangement of the above equation, i.e.,

$$g = h v \; /$$

using the magnetic field and the frequency of the spectrometer. Since h, v, and ß should not change during an experiment, g values decrease as B increases. The concept of g can be roughly equated to that of chemical shift in NMR.

3.8.1.2 Instrumentation

EPR spectroscopy can be carried out by either 1) varying the magnetic field and holding the frequency constant or 2) varying the frequency and holding the magnetic field constant (as is the case for NMR spectroscopy). Commercial EPR spectrometers typically vary the magnetic field and holding the frequency constant, opposite of NMR spectrometers. The majority of EPR spectrometers are in the range of 8-10 GHz (X-band), though there are spectrometers which work at lower and higher fields: 1-2 GHz (L-band) and 2-4 GHz (S-band), 35 GHz (Q-band) and 95 GHz (W-band).
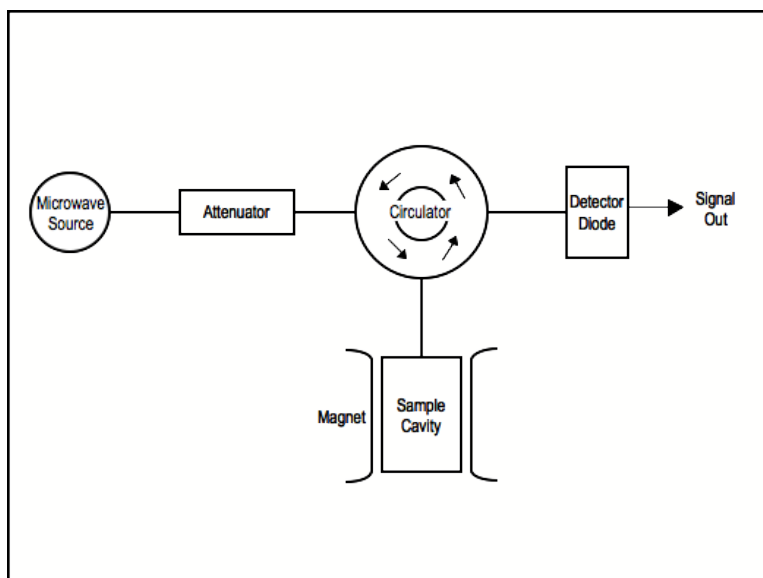

Figure 3.151: Block diagram of a typical EPR spectrometer.

EPR spectrometers work by generating microwaves from a source (typically a klystron), sending them through an attenuator, and passing them on to the sample, which is located in a microwave cavity (Figure 3.151). Microwaves reflected back from the cavity are routed to the detector diode, and the signal comes out as a decrease in current at the detector analogous to absorption of microwaves by the sample.

Samples for EPR can be gases, single crystals, solutions, powders, and frozen solutions. For solutions, solvents with high dielectric constants are not advisable, as they will absorb microwaves. For frozen solutions, solvents that will form a glass when frozen are preferable. Good glasses are formed from solvents with low

symmetry and solvents that do not hydrogen bond. Drago provides an extensive list of solvents that form good glasses.

EPR spectra are generally presented as the first derivative of the absorption spectra for ease of interpretation. An example is given in Figure 3.152.
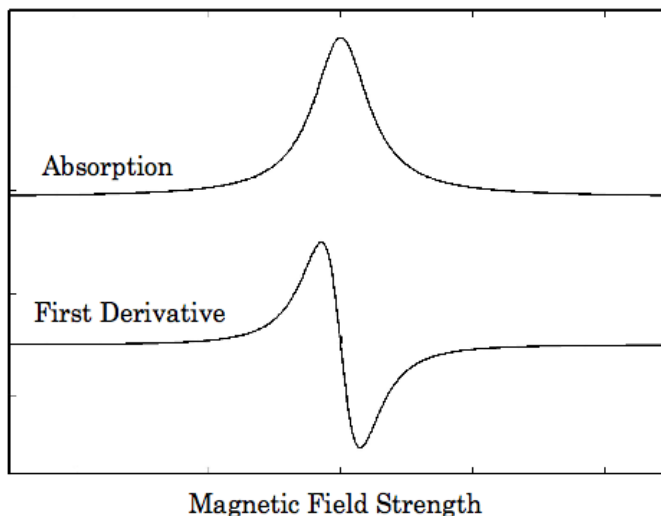

Figure 3.152: Example of first and second derivative EPR spectrum.

Magnetic field strength is generally reported in units of Gauss or mTesla. Often EPR spectra are very complicated, and analysis of spectra through the use of computer programs is usual. There are computer programs that will predict the EPR spectra of compounds with the input of a few parameters.

3.8.1.3 Factors that affect EPR spectra

3.8.1.3.1 Hyperfine coupling

Hyperfine coupling in EPR is analogous to spin-spin coupling in NMR. There are two kinds of hyperfine coupling: 1) coupling of the electron magnetic moment to the magnetic moment of its own nucleus; and 2) coupling of the electron to a nucleus of a different atom, called super hyperfine splitting. Both types of hyperfine coupling cause a splitting of the spectral lines with intensities following Pascal's triangle for $I = 1/2$ nuclei, similar to J-coupling in NMR. A simulated spectrum of the methyl radical is shown in Figure 3.153. The line is split equally by the three hydrogens giving rise to four lines of intensity 1:3:3:1 with hyperfine coupling constant a.
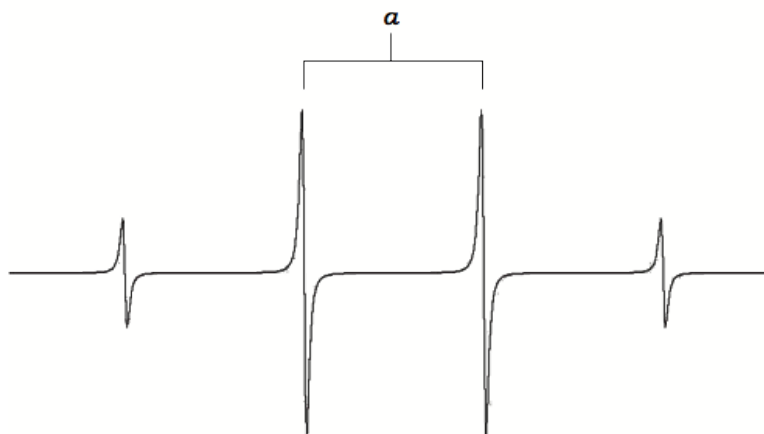
Figure 3.153: Simulated spectrum of CH$_3$ radical with hyperfine coupling constant a.

The hyperfine splitting constant, known as a, can be determined by measuring the distance between each of the hyperfine lines. This value can be converted into Hz (A) using the g value in the equation:

hA = g

In the specific case of Cu(II), the nuclear spin of Cu is I = 3/2, so the hyperfine splitting would result in four lines of intensity 1:1:1:1. Similarly, super hyperfine splitting of Cu(II) ligated to four symmetric I = 1 nuclei, such as ^{14}N, would yield nine lines with intensities would be 1:8:28:56:70:56:28:8:1.

3.8.1.3.2 Anisotropy

The g factor of many paramagnetic species, including Cu(II), is anisotropic, meaning that it depends on its orientation in the magnetic field. The g factor for anisotropic species breaks down generally into three values of g following a Cartesian coordinate system which is symmetric along the diagonal: gx, gy, and gz. There are four limits to this system:

  i) When $gx = gy = gz$ the spectrum is considered to be isotropic, and is not dependent on orientation in the magnetic field.
  ii) When $gx = gy > gz$ the spectrum is said to be axial, and is elongated along the z-axis. The two equivalent g values are known as $g_\perp$ while the singular value is known as $g_\parallel$. It exhibits a small peak at low field and a large peak at high field.
  iii) When $gx = gy < gz$ the spectrum is also said to be axial, but is shortened in the xy plane. It exhibits a large peak at low field and a small peak at high field.
  iv) When $gx \neq gy \neq gz$ the spectrum is said to be rhombic, and shows three large peaks corresponding to the different components of g.

Condition ii corresponds to Cu(II) in a square planar geometry with the unpaired electron in the $d_{x^2-y^2}$ orbital. Where there is also hyperfine splitting involved, g is defined as being the weighted average of the lines.

3.8.1.4 Bibliography

- R. S. Drago, *Physical Methods for Chemists*. 2nd edition, Saunders College Publishing, Mexico (1992).

- G. Palmer, In *Physical Methods in Bioinorganic Chemistry Spectroscopy and Magnetism*. Ed. L. Que, University Science Books, Sausalito, CA (2000).
- P. H. Rieger, *Electron Spin Resonance: Analysis and Interpretation*. Royal Society of Chemistry, Cambridge, UK, (2007).
- J. Weil, J. Bolton, and J. Wertz, *Electron Paramagnetic Resonance: Elemental Theory and Practical Applications*, John Wiley and Sons, New York (1994).

3.8.2 Electron Paramagnetic Resonance Spectroscopy of Copper(II) Compounds[29]

3.8.2.1 Copper(II) Compounds

Copper compounds play a valuable role in both synthetic and biological chemistry. Copper catalyzes a vast array of reactions, primarily oxidation-reduction reactions which make use of the $Cu(I)/Cu(II)$ redox cycle. Copper is found in the active site of many enzymes and proteins, including the oxygen carrying proteins called hemocyanins.

Common oxidation states of copper include the less stable copper(I) state, Cu^+; and the more stable copper(II) state, Cu^{2+}. Copper (I) has a d^{10} electronic configuration with no unpaired electrons, making it undetectable by EPR. The d^9 configuration of Cu^{2+} means that its compounds are paramagnetic making EPR of Cu(II) containing species a useful tool for both structural and mechanistic studies. Two literature examples of how EPR can provide insight into the mechanisms of reactivity of Cu(II) are discussed herein.

Copper (II) centers typically have tetrahedral, or axially elongated octahedral geometry. Their spectra are anisotropic and generally give signals of the axial or orthorhombic type. From EPR spectra of copper (II) compounds, the coordination geometry can be determined. An example of a typical powder Cu(II) spectrum is shown in Figure 3.154.
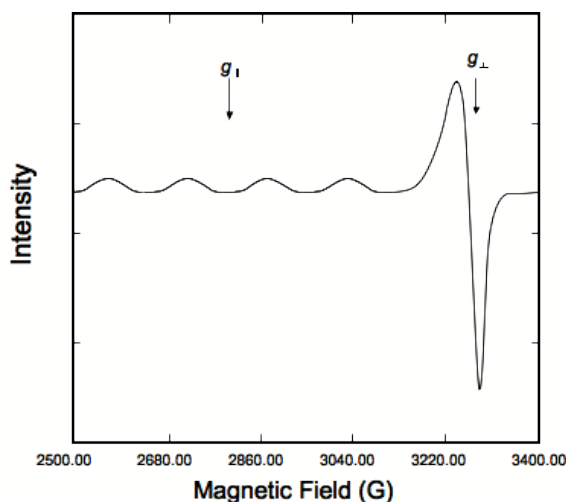

Figure 3.154: Typical axial EPR spectrum for a Cu(II) compound.

[29]This content is available online at <http://cnx.org/content/m22507/1.2/>.

The spectrum above shows four absorption-like peaks corresponding to $g_{\parallel}$ indicating coordination to four identical atoms, most likely nitrogen. There is also an asymmetric derivative peak corresponding to $g_{\perp}$ at higher field indicating elongation along the z axis.

3.8.2.1.1 Determination of an intermediate

The reactivity and mechanism of Cu(II)-peroxy systems was investigated by studying the decomposition of the Cu(II) complex **1** with EPR as well as UV-Vis and Raman spectroscopy. The structure (Figure 3.155) and EPR spectrum Figure 3.156 of **1** are given. It was postulated that decomposition of **1** may go through intermediates LCu(II)OOH, LCu(II)OO•, or LCu(II)O• where L = ligand.
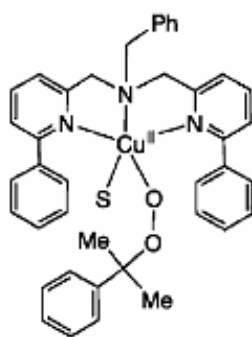
Figure 3.155: Structure of **1**, Cu(II) compound under investigation S = CH$_3$CN
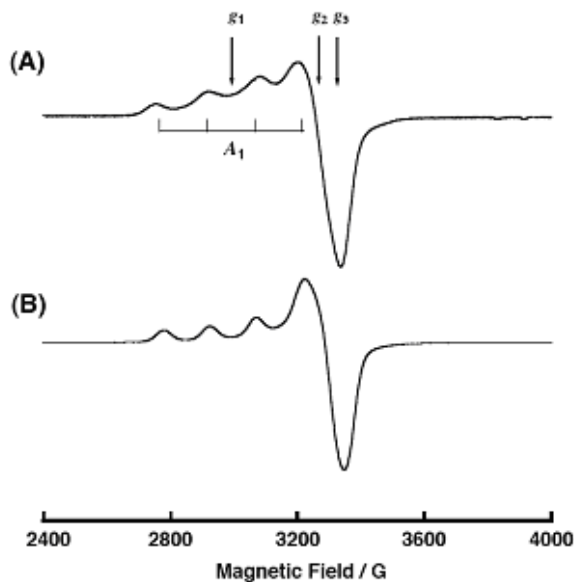
Figure 3.156: EPR spectrum of **1** in CH_3CN at -150 °C showing g values of g_1= 2.250, g_2 = 2.065, g_3 = 2.030, and hyperfine coupling constant A_1 = 160 G, A_2 = 7 G, and A_3 = 5 G. A. Kunishita, H. Ishimaru, S. Nakashima, T. Ogura, and S. Itoh, *J. Am. Chem. Soc.*, 2008, **130**, 4244. Copyright American Chemical Society (2008).

To determine the intermediate, a common radical trap 5,5-dimethyl-1-pyrroline-N-oxide (DMPO) was added. A 1:1 complex of intermediate and DMPO was isolated, and given the possible structure **2** (Figure 3.157), which is shown along with its EPR spectrum (Figure 3.158).
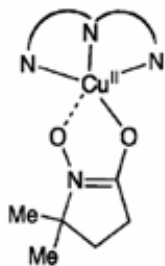
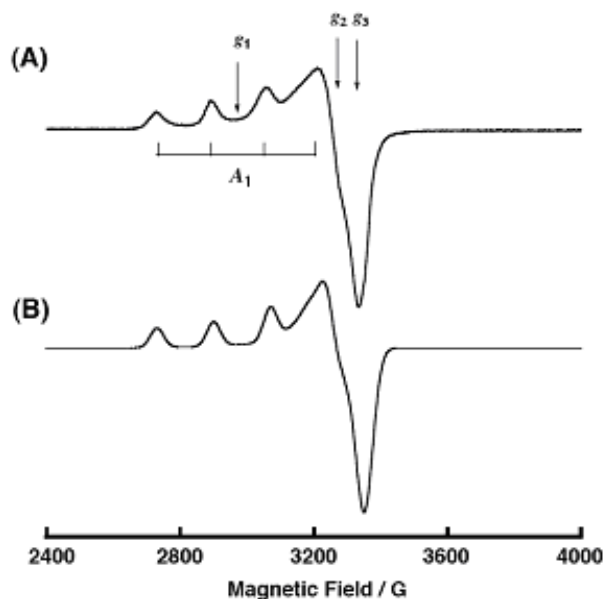**Figure 3.157:** Proposed structure **2**, S = CH_3CN.

Figure 3.158: EPR spectrum of **1** in CH$_3$CN at -150 °C showing g values of $g_1 = 2.250$, $g_2 = 2.065$, $g_3 = 2.045$, and hyperfine coupling constant A$_1$ = 170 G, A$_2$ = 25 G, and A$_3$ = 30 G. A. Kunishita, H. Ishimaru, S. Nakashima, T. Ogura, and S. Itoh, *J. Am. Chem. Soc.*, 2008, **130**, 4244. Copyright American Chemical Society (2008).

The EPR data show similar though different spectra for Cu(II) in each compound, indicating a similar coordination environment − elongated axial, and most likely a LCu(II)O• intermediate.

3.8.2.1.2 Determination of a catalytic cycle

The mechanism of oxidizing alcohols to aldehydes using a Cu(II) catalyst, TEMPO, and O$_2$ was investigated using EPR. A proposed mechanism is given in Figure 3.159.
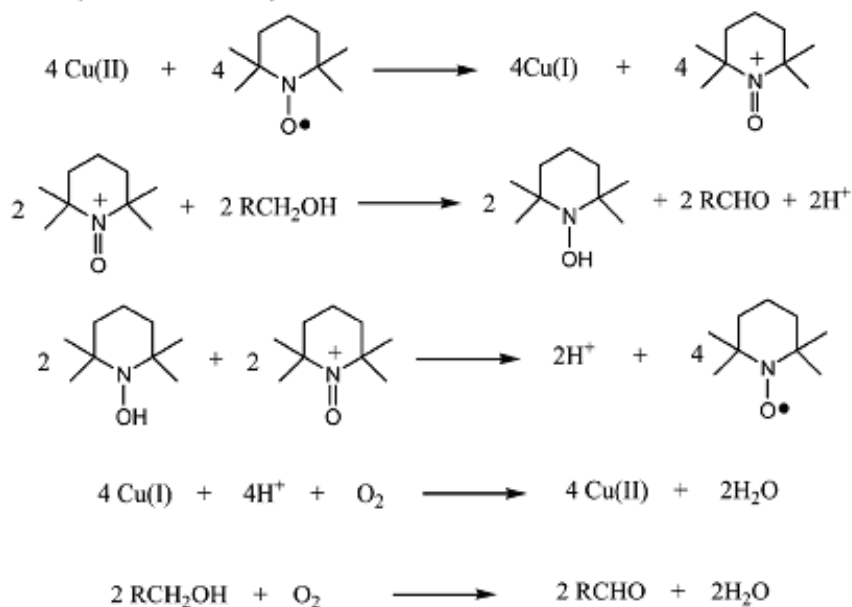
Figure 3.159: Proposed mechanism for the Cu(II) mediated oxidation of alcohols to aldehydes with TEMPO and O_2. M. Contel, P. R. Villuendas, J. Fernández-Gallardo, P. Alonso, J. M. Vincent, and R. Fish, *Inorg. Chem.*, 2005, **44**, 9771. Copyright American Chemical Society (2005).

EPR studies were conducted during the reaction by taking aliquots at various time points and immediately freezing the samples for EPR analysis. The resulting spectra are shown in Figure 3.160.
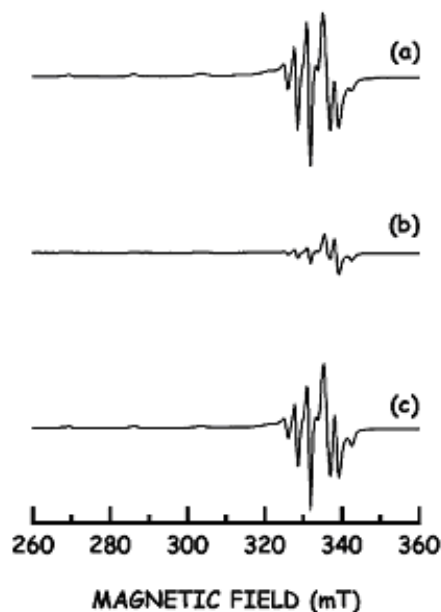
Figure 3.160: EPR spectra of reaction at (a) 1.2 h (b) 4 h (c) 8 h, M. Contel, P. R. Villuendas, J. Fernández-Gallardo, P. Alonso, J. M. Vincent, and R. Fish, *Inorg. Chem.*, 2005, **44**, 9771. Copyright American Chemical Society (2005).

The EPR spectrum (a) in Figure 6, after 1.2 hours shows a signal for TEMPO at g = 2.006 as well as a signal for Cu(II) with $g_{\parallel} = 2.26$, $g_{\perp} = 2.06$, $A_{\parallel} = 520$ MHz, and $A_{\perp} < 50$ MHz. After 4 hours, the signal for Cu(II) is no longer in the reaction mixture, and the TEMPO signal has decreased significantly. Suggesting that all the Cu(II) has been reduced to Cu(I) and the majority of TEMPO has been oxidized. After 8 hours, the signals for both Cu(II) and TEMPO have returned indicating regeneration of both species. In this way, EPR evidence supports the proposed mechanism.

3.8.2.1.3 Bibliography

- M. Contel, P. R. Villuendas, J. Fernández-Gallardo, P. Alonso, J. M. Vincent, and R. Fish, *Inorg. Chem.*, 2005, **44**, 9771.
- A. Kunishita, H. Ishimaru, S. Nakashima, T. Ogura, S. Itoh, *J. Am. Chem. Soc.*, 2008, **130**, 4244.
- G. Palmer, In *Physical Methods in Bioinorganic Chemistry Spectroscopy and Magnetism*. Ed. L. Que, University Science Books: Sausalito, CA (2000).
- J. Pilbrow, *Transition Ion Electron Paramagnetic Resonance*, Clarenden Press, Oxford (1990).
- J. Weil, J. Bolton, and J. Wertz, *Electron Paramagnetic Resonance: Elemental Theory and Practical Applications* John Wiley and Sons: New York (1994).

3.9 X-ray Photoelectron Spectroscopy

3.9.1 XPS of Carbon Nanomaterials[30]

3.9.1.1 Introduction

X-ray photoelectron spectroscopy (XPS), also called electron spectroscopy for chemical analysis (ESCA), is a method used to determine the elemental composition of a material's surface. It can be further applied to determine the chemical or electronic state of these elements.

The photoelectric effect is the ejection of electrons from the surface of a material upon exposure to electromagnetic radiation of sufficient energy. Electrons emitted have characteristic kinetic energies proportional to the energy of the radiation, according to (3.23), where KE is the kinetic energy of the electron, h is Planck's constant, ν is the frequency of the incident radiation, E_b is the ionization, or binding, energy, and ϕ is the work function. The work function is a constant which is dependent upon the spectrometer.

$$KE = h\nu - E_b - \varphi$$

(3.23)

In photoelectron spectroscopy, high energy radiation is used to expel core electrons from a sample. The kinetic energies of the resulting core electrons are measured. Using the equation with the kinetic energy and known frequency of radiation, the binding energy of the ejected electron may be determined. By Koopman's theorem, which states that ionization energy is equivalent to the negative of the orbital energy, the energy of the orbital from which the electron originated is determined. These orbital energies are characteristic of the element and its state.

3.9.1.2 Basics of XPS

3.9.1.2.1 Sample preparation

As a surface technique, samples are particularly susceptible to contamination. Furthermore, XPS samples must be prepared carefully, as any loose or volatile material could contaminate the instrument because of the ultra-high vacuum conditions. A common method of XPS sample preparation is embedding the solid sample into a graphite tape. Samples are usually placed on 1 x 1 cm or 3 x 3 cm sheets.

3.9.1.2.2 Experimental set-up

Monochromatic aluminum ($h\nu$ = 1486.6 eV) or magnesium ($h\nu$ = 1253.6 eV) K_α X-rays are used to eject core electrons from the sample. The photoelectrons ejected from the material are detected and their energies measured. Ultra-high vacuum conditions are used in order to minimize gas collisions interfering with the electrons before they reach the detector.

3.9.1.2.3 Measurement specifications

XPS analyzes material between depths of 1 and 10 nm, which is equivalent to several atomic layers, and across a width of about 10 μm. Since XPS is a surface technique, the orientation of the material affects the spectrum collected.

3.9.1.2.4 Data collection

X-ray photoelectron (XP) spectra provide the relative frequencies of binding energies of electrons detected, measured in electron-volts (eV). Detectors have accuracies on the order of ±0.1 eV. The binding energies are used to identify the elements to which the peaks correspond. XPS data is given in a plot of intensity versus binding energy. Intensity may be measured in counts per unit time (such as counts per second, denoted c/s). Often, intensity is reported as arbitrary units (arb. units), since only relative intensities provide relevant

---

[30]This content is available online at <http://cnx.org/content/m34549/1.2/>.

information. Comparing the areas under the peaks gives relative percentages of the elements detected in the sample. Initially, a survey XP spectrum is obtained, which shows all of the detectable elements present in the sample. Elements with low detection or with abundances near the detection limit of the spectrometer may be missed with the survey scan. Figure 3.161 shows a sample survey XP scan of fluorinated double-walled carbon nanotubes (DWNTs).
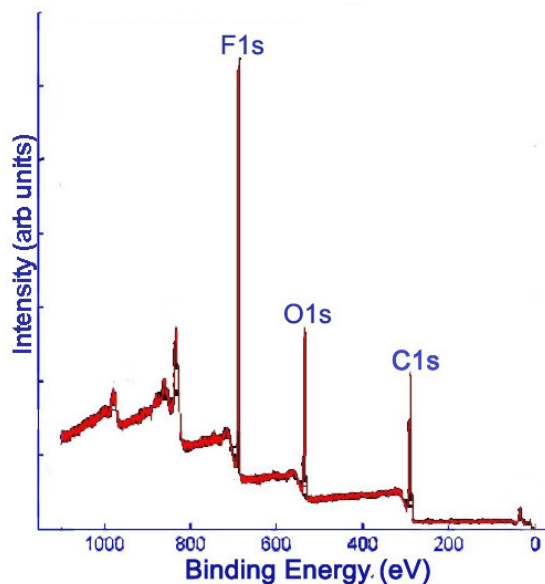

Figure 3.161: Survey XP spectrum of F-DWNTs (O. Kuznetsov, Rice University).

Subsequently, high resolution scans of the peaks can be obtained to give more information. Elements of the same kind in different states and environments have slightly different characteristic binding energies. Computer software is used to fit peaks within the elemental peak which represent different states of the same element, commonly called deconvolution of the elemental peak. Figure 3.162 and Figure 3.163 show high resolutions scans of C1s and F1s peaks, respectively, from Figure 3.161, along with the peak designations.
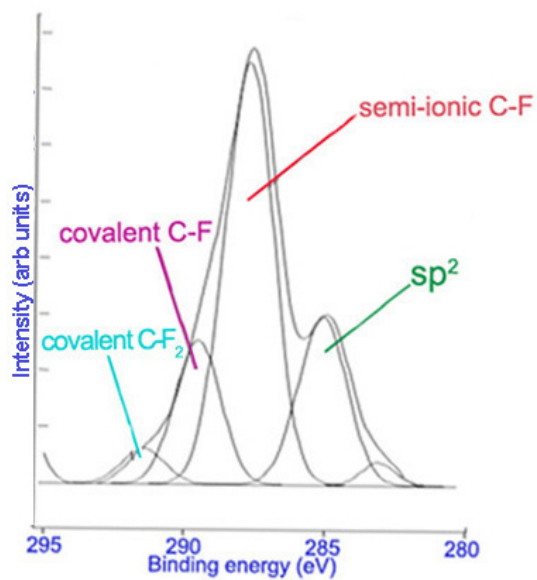
Figure 3.162: Deconvoluted high resolution C1s spectrum of F-DWNTs (O. Kuznetsov, Rice University).
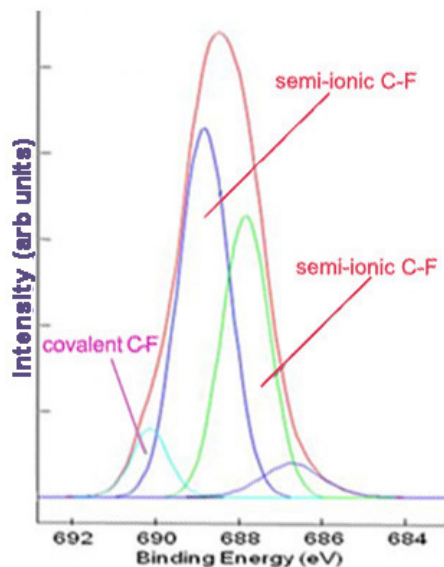
Figure 3.163: Deconvoluted high resolution F1s spectrum of F-DWNTs (O. Kuznetsov, Rice University).

3.9.1.2.5 Limitations

Both hydrogen and helium cannot be detected using XPS. For this reason, XPS can provide only relative, rather than absolute, ratios of elements in a sample. Also, elements with relatively low atomic percentages close to that of the detection limit or low detection by XPS may not be seen in the spectrum. Furthermore, each peak represents a distribution of observed binding energies of ejected electrons based on the depth of the atom from which they originate, as well as the state of the atom. Electrons from atoms deeper in the sample must travel through the above layers before being liberated and detected, which reduces their kinetic energies and thus increases their apparent binding energies. The width of the peaks in the spectrum consequently depends on the thickness of the sample and the depth to which the XPS can detect; therefore, the values obtained vary slightly depending on the depth of the atom. Additionally, the depth to which XPS can analyze depends on the element being detected.

High resolution scans of a peak can be used to distinguish among species of the same element. However, the identification of different species is discretionary. Computer programs are used to deconvolute the elemental peak. The peaks may then be assigned to particular species, but the peaks may not correspond with species in the sample. As such, the data obtained must be used cautiously, and care should be taken to avoid over-analyzing data.

3.9.1.3 XPS for carbon nanomaterials

Despite the aforementioned limitations, XPS is a powerful surface technique that can be used to accurately detect the presence and relative quantities of elements in a sample. Further analysis can provide information about the state and environment of atoms in the sample, which can be used to infer information about the surface structure of the material. This is particularly useful for carbon nanomaterials, in which surface

structure and composition greatly influence the properties of the material. There is much research interest in modifying carbon nanomaterials to modulate their properties for use in many different applications.

3.9.1.3.1 Sample preparation

Carbon nanomaterials present certain issues in regard to sample preparation. The use of graphite tape is a poor option for carbon nanomaterials because the spectra will show peaks from the graphite tape, adding to the carbon peak and potentially skewing or overwhelming the data. Instead, a thin indium foil (between 0.1 and 0.5 mm thick) is used as the sample substrate. The sample is simply pressed onto a piece of the foil.

3.9.1.4 Analysis and applications for carbon nanomaterials

3.9.1.4.1 Chemical Speciation

The XP survey scan is an effective way to determine the identity of elements present on the surface of a material, as well as the approximate relative ratios of the elements detected. This has important implications for carbon nanomaterials, in which surface composition is of greatest importance in their uses. XPS may be used to determine the purity of a material. For example, nanodiamond powder is a created by detonation, which can leave nitrogenous groups and various oxygen containing groups attached to the surface. Figure 3.164 shows a survey scan of a nanodiamond thin film with the relative atomic percentages of carbon, oxygen, and nitrogen being 91.25%, 6.25%, and 1.7%, respectively. Based on the XPS data, the nanodiamond material is approximately 91.25% pure.
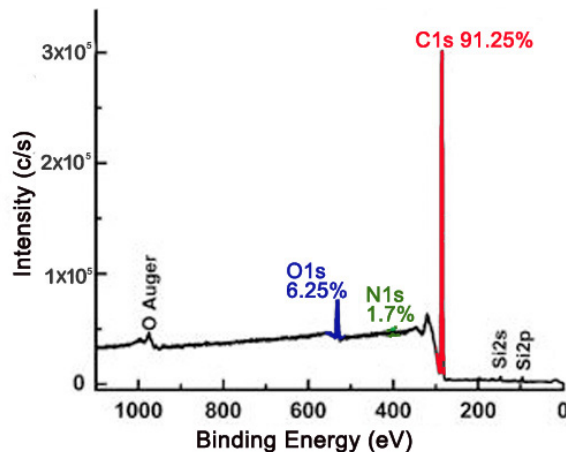

Figure 3.164: Survey XPS of a nanodiamond thin film. Adapted from F. Y. Xie, W. G. Xie, J. Chen, X. Liu, D. Y. Lu, and W. H. Zhang, *J. Vac. Sci. Tech. B*, 2008, **26**, 102.

XPS is a useful method to verify the efficacy of a purification process. For example, high-pressure CO conversion single-walled nanotubes (HiPco SWNTs) are made using iron as a catalyst. Figure 3.165 shows the Fe2p XP spectra for pristine and purified HiPco SWNTs.
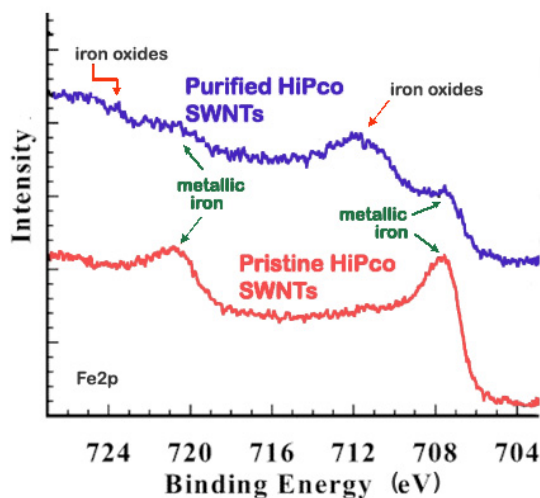
Figure 3.165: High resolution scan of Fe2p peak for pristine and purified HiPco SWNTs. Adapted with permission from C. M. Yang, H. Kanoh, K. Kaneko, M. Yudasaka, and S. Iijima, *J. Phys. Chem. B*, 2002, **106**, 8994. Copyright: American Chemical Society (2002).

For this application, XPS is often done in conjunction with thermogravimetric analysis (TGA), which measures the weight lost from a sample at increasing temperatures. TGA data serves to corroborate the changes observed with the XPS data by comparing the percentage of weight loss around the region of the impurity suspected based on the XP spectra. The TGA data support the reduction in iron content with purification suggested by the XP spectra above, for the weight loss at temperatures consistent with iron loss decreases from 27% in pristine SWNTs to 18% in purified SWNTs. Additionally, XPS can provide information about the nature of the impurity. In Figure 3.165, the Fe2p spectrum for pristine HiPco SWNTs shows two peaks characteristic of metallic iron at 707 and 720 eV. In contrast, the Fe2p spectrum for purified HiPco SWNTs also shows two peaks at 711 and 724 eV, which are characteristic of either Fe_2O_3 or Fe_3O_4. In general, the atomic percentage of carbon obtained from the XPS spectrum is a measure of the purity of the carbon nanomaterials.

3.9.1.4.2 Bonding and functional groups

XP spectra give evidence of functionalization and can provide insight into the identity of the functional groups. Carbon nanomaterials provide a versatile surface which can be functionalized to modulate their properties. For example, the sodium salt of phenyl sulfonated SWNTs is water soluble. In the XP survey scan of the phenyl sulfonated SWNTs, there is evidence of functionalization owing to the appearance of the S2p peak. Figure 3.166 shows the survey XP spectrum of phenyl sulfonated SWNTs.
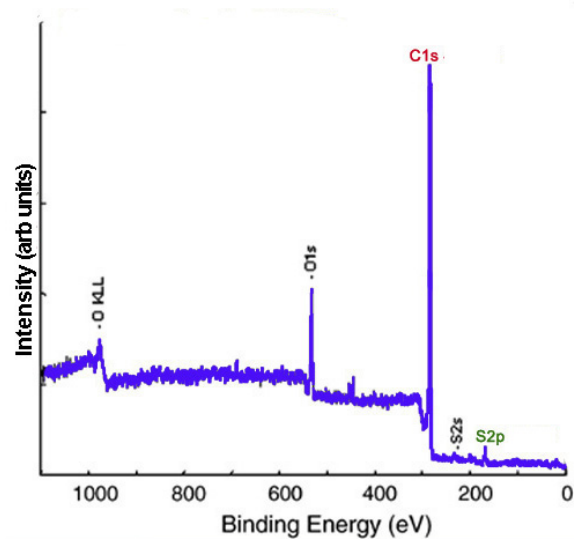
Figure 3.166: Survey XP spectrum of phenyl sulfonated SWNTs. Adapted with permission from F. Liang, J. M. Beach, P. K. Rai, W. H. Guo, R. H. Hauge, M. Pasquali, R. E. Smalley, and W. E. Billups, *Chem. Mater.*, 2006, **18**, 1520. Copyright: American Chemical Society (2006).

The survey XP spectrum of the sodium salt shows a Na1s peak (Figure 3.167) and the high resolution scans of Na1s and S2p show that the relative atomic percentages of Na1s and S2p are nearly equal (Figure 3.168), which supports the formation of the sodium salt.
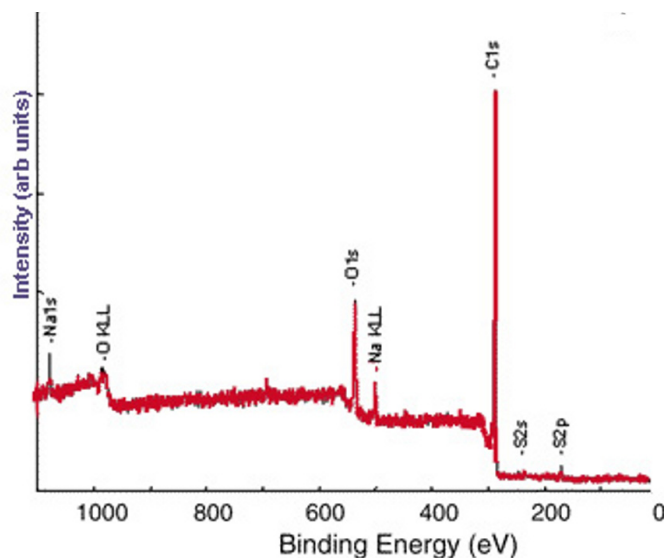
Figure 3.167: Survey XP spectrum of phenyl sulfonated SWNTs. Adapted with permission from F. Liang, J. M. Beach, P. K. Rai, W. H. Guo, R. H. Hauge, M. Pasquali, R. E. Smalley, and W. E. Billups, *Chem. Mater.*, 2006, **18**, 1520. Copyright: American Chemical Society (2006).
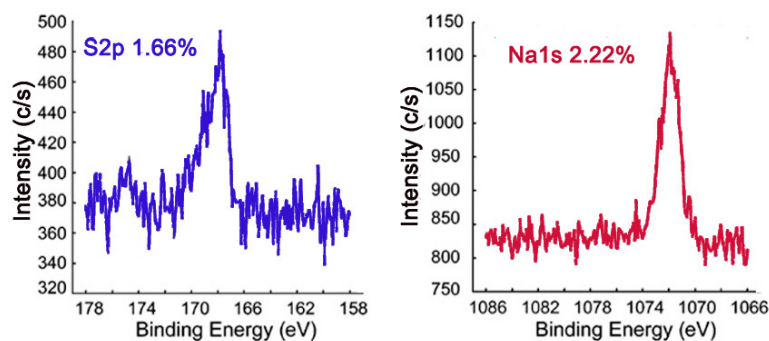

Figure 3.168: High resolution S2p (left) and Na1s (right) XP spectra of phenyl sulfonated SWNTs. Adapted with permission from F. Liang, J. M. Beach, P. K. Rai, W. H. Guo, R. H. Hauge, M. Pasquali, R. E. Smalley, and W. E. Billups, *Chem. Mater.*, 2006, **18**, 1520. Copyright: American Chemical Society (2006).

3.9.1.4.3 Further characterization

High resolution scans of each of the element peaks of interest can be obtained to give more information about the material. This is a way to determine with high accuracy the presence of elements as well as relative ratios of elements present in the sample. This can be used to distinguish species of the same element in different chemical states and environments, such as through bonding and hybridization, present in the material. The distinct peaks may have binding energies that differ slightly from that of the convoluted elemental peak. Assignment of peaks can be done using XPS databases, such as that produced by NIST[31] . The ratios of the intensities of these peaks can be used to determine the percentage of atoms in a particular state. Discrimination between and identity of elements in different states and environments is a strength of XPS that is of particular interest for carbon nanomaterials.

3.9.1.4.3.1 Hybridization

The hybridization of carbons influences the properties of a carbon nanomaterial and has implications in its structure. XPS can be used to determine the hybridization of carbons on the surface of a material, such as graphite and nanodiamond. Graphite is a carbon material consisting of sp^2 carbons. Thus, theoretically the XPS of pure graphite would show a single C1s peak, with a binding energy characteristic of sp^2 carbon (around 284.2 eV). On the other hand, nanodiamond consists of sp^3 bonded carbons. The XPS of nanodiamond should show a single C1s peak, with a binding energy characteristic of sp^3 carbon (around 286 eV). The ratio of the sp^2 and sp^3 peaks in the C1s spectrum gives the ratio of sp^2 and sp^3 carbons in the nanomaterial. This ratio can be altered and compared by collecting the C1s spectra. For example, laser treatment of graphite creates diamond-like material, with more sp^3 character when a higher laser power is used. This can be observed in Figure 3.169, in which the C1s peak is broadened and shifted to higher binding energies as increased laser power is applied.
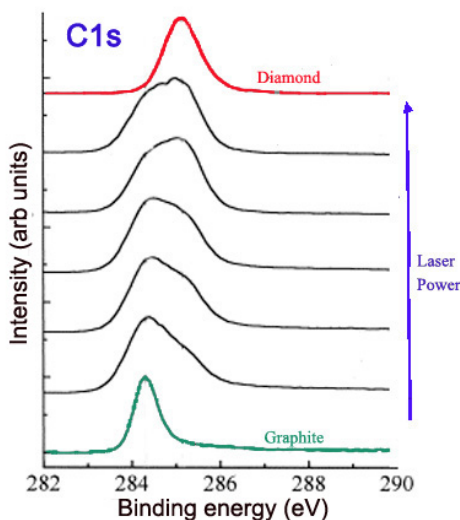

Figure 3.169: C1s high resolution XP spectra of graphite, nanodiamond, and graphite samples with increasing laser power treatment. Adapted from P. Merel, M. Tabbal, M. Chaker, S. Moisa, and J. Margot, *Appl. Surf. Sci.*, 1998, **136**, 105.

---

[31]http://srdata.nist.gov/xps/Default.aspx

Alternatively, annealing nanodiamond thin films at very high temperatures creates graphitic layers on the nanodiamond surface, increasing sp^2 content. The extent of graphitization increases with the temperature at which the sample is annealed, as shown in Figure 3.170.
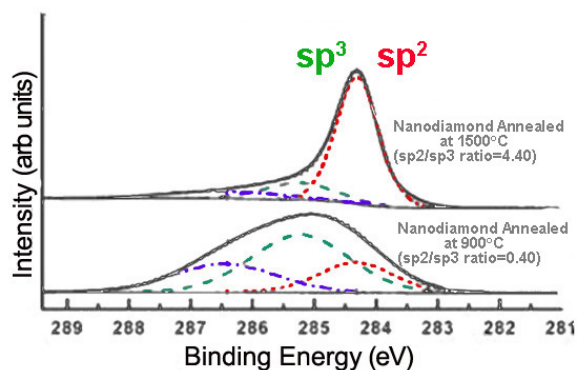

Figure 3.170: Deconvoluted high resolution C1s XP spectra for annealed nanodiamond. Adapted from F. Y. Xie, W. G. Xie, J. Chen, X. Liu, D. Y. Lu, and W. H. Zhang, *J. Vac. Sci. Tech. B*, 2008, **26**, 102.

3.9.1.4.3.2 Reaction completion

Comparing the relative intensities of various C1s peaks can be powerful in verifying that a reaction has occurred. Fluorinated carbon materials are often used as precursors to a broad range of variously functionalized materials. Reaction of fluorinated SWNTs (F-SWNTs) with polyethyleneimine (PEI) leads to decreases in the covalent carbon-fluoride C1s peak, as well as the evolution of the amine C1s peak. These changes are observed in the C1s spectra of the two samples (Figure 3.171).
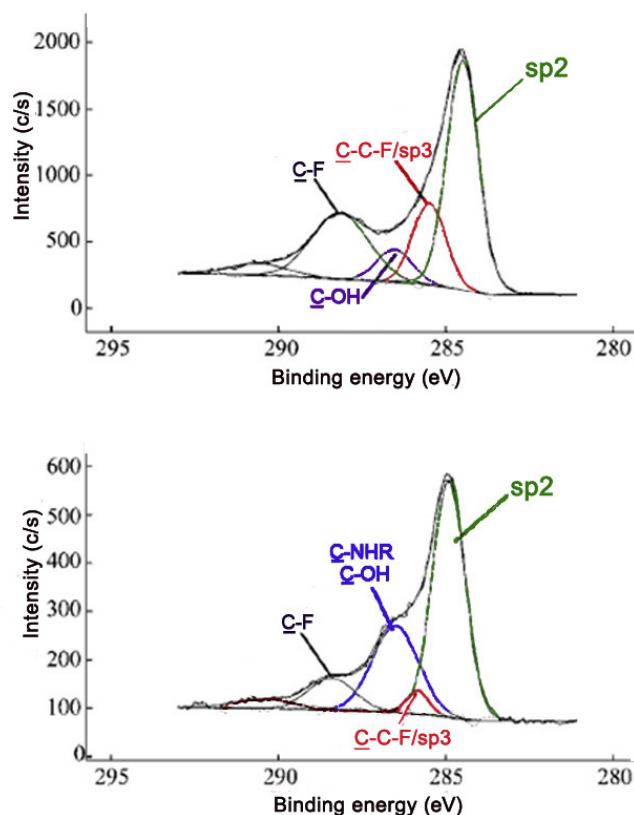
Figure 3.171: High resolution C1s XP spectra of F-SWNTs (top) and PEI-SWNTs (bottom). Adapted with permission from E. P. Dillon, C. A. Crouse, and A. R. Barron, *ACS Nano*, 2008, **2**, 156. Copyright: American Chemical Society (2008).

3.9.1.4.3.3 Nature and extent of functionalization

XPS can also be applied to determine the nature and extent of functionalization. In general, binding energy increases with decreasing electron density about the atom. Species with more positive oxidation states have higher binding energies, while more reduced species experience a greater degree of shielding, thus increasing the ease of electron removal.

The method of fluorination of carbon materials and such factors as temperature and length of fluorination affect the extent of fluoride addition as well as the types of carbon-fluorine bonds present. A survey scan can be used to determine the amount of fluorine compared to carbon. High resolution scans of the C1s and F1s peaks can also give information about the proportion and types of bonds. A shift in the peaks, as well as changes in peak width and intensity, can be observed in spectra as an indication of fluorination of graphite. Figure 3.172 shows the Cls and F1s spectra of samples containing varying ratios of carbon to fluorine.
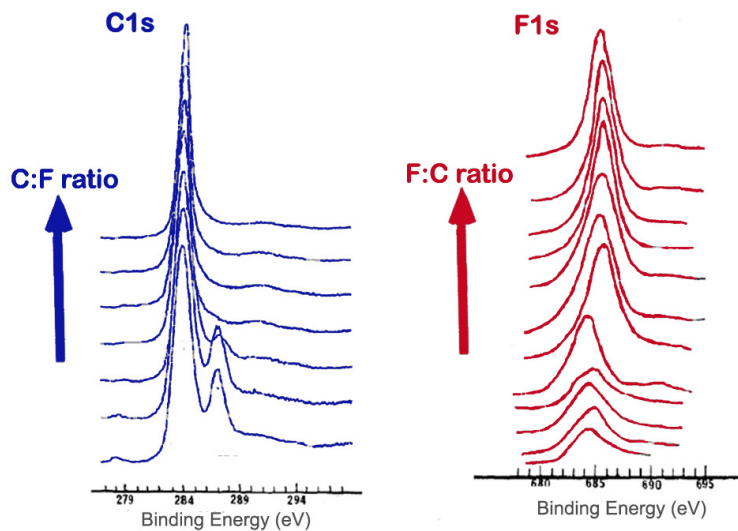
Figure 3.172: C1s and F1s high resolution XP spectra for graphite fluorides. Adapted from I. Palchan, M. Crespin, H. Estrade-Szwarckopf, and B. Rousseau. *Chem. Phys. Lett.*, 1989, **157**, 321.

Furthermore, different carbon-fluorine bonds show characteristic peaks in high resolution C1s and F1s spectra. The carbon-fluorine interactions in a material can range from ionic to covalent. Covalent carbon-fluorine bonds show higher core electron binding energies than bonds more ionic in character. The method of fluorination affects the nature of the fluorine bonds. Graphite intercalation compounds are characterized by ionic carbon-fluorine bonding. Figure 3.173 shows the F1s spectra for two fluorinated exfoliated graphite samples prepared with different methods.
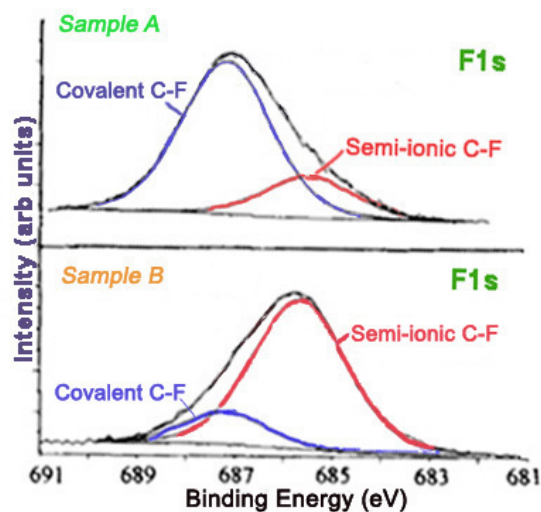
Figure 3.173: High resolution F1s XP spectra of two fluorinated exfoliated graphite samples. Adapted from A. Tressaud, F. Moguet, S. Flandrois, M. Chambon, C. Guimon, G. Nanse, E. Papirer, V. Gupta, and O.P. Bahl. *J. Phys. Chem. Solids*, 1996, **57**, 745.

Also, the peaks for carbons attached to a single fluorine atom, two fluorine atoms, and carbons attached to fluorines have characteristic binding energies. These peaks are seen in that C1s spectra of F- and PEI-SWNTs shown in Figure 3.174.
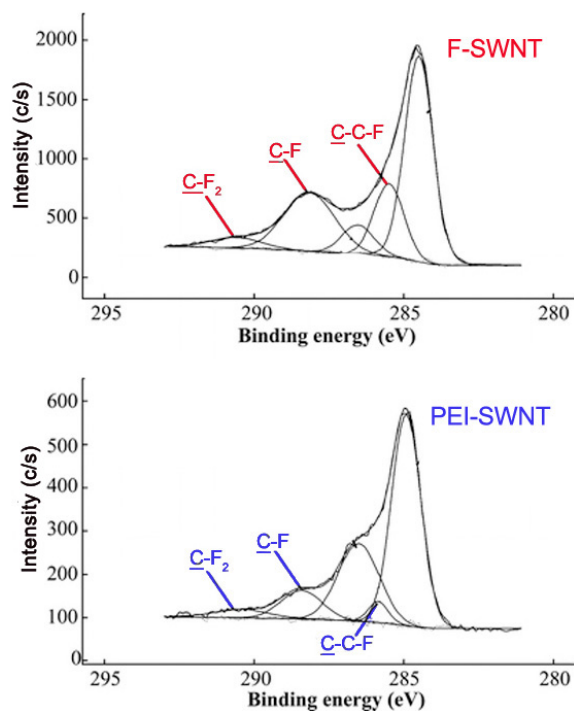
Figure 3.174: High resolution C1s XP spectra of F-SWNTs (top) and PEI-SWNTs (bottom). Adapted with permission from E. P. Dillon, C. A. Crouse, and A. R. Barron, *ACS Nano*, 2008, **2**, 156. Copyright: American Chemical Society (2008).

Table 3.24 lists various bonds and functionalities and the corresponding C1s binding energies, which may be useful in assigning peaks in a C1s spectrum, and consequently in characterizing the surface of a material.

Bond/Group	Binding Energy (eV)
C-C	**284.0-286.0**
C-C (sp^2)	284.3-284.6
C-C (sp^3)	285.0-286.0
C-N	**285.2-288.4**
C-NR$_2$ (amine)	285.5-286.4
O=C-NH (amide)	287.9-288.6
-C≡N (nitrile)	266.3-266.8
C-O	**286.1-290.0**
O=C-OH (carboxyl)	288.0-289.4
-C-O (epoxy)	286.1-287.1
-C-OH (hydroxyl)	286.4-286.7
-C-O-C- (ether)	286.1-288.0
-C=O (aldehyde/ketone)	287.1-288.1
C-F	**287.0-293.4**
-C-F (covalent)	287.7-290.2
-C-F (ionic)	287.0-287.4
C-C-F	286.0-287.7
C-F$_2$	291.6-292.4
C-F$_3$	292.4-293.4
C-S	**285.2-287.5**
C-Cl	**287.0-287.2**

Table 3.24: Summary of selected C1s binding energies.

3.9.1.4.4 Conclusion

X-ray photoelectron spectroscopy is a facile and effective method for determining the elemental composition of a material's surface. As a quantitative method, it gives the relative ratios of detectable elements on the surface of the material. Additional analysis can be done to further elucidate the surface structure. Hybridization, bonding, functionalities, and reaction progress are among the characteristics that can be inferred using XPS. The application of XPS to carbon nanomaterials provides much information about the material, particularly the first few atomic layers, which are most important for the properties and uses of carbon nanomaterials.

3.9.1.5 Bibliography

- J. Bockris, *Modern Electrochemistry 2A*, 2nd ed., Springer (2001).
- E. P. Dillon, C. A. Crouse, and A. R. Barron, *ACS Nano*, 2008, **2**, 156.
- Y. G. Gogotsi, and I. V. Uvarova, *Nanostructured materials and coatings for biomedical and sensor applications,* Kluwer Academic Publishing (2003).
- F. Liang, J. M. Beach, P. K. Rai, W. H. Guo, R. H. Hauge, M. Pasquali, R. E. Smalley, and W. E. Billups, *Chem. Mater.*, 2006, **18**, 1520.

- P. Merel, M. Tabbal, M. Chaker, S. Moisa, and J. Margot, *Appl. Surf. Sci.*, 1998, **136**, 105.
- T. Nakajima, *Graphite fluorides and carbon-fluorine compounds*, CRC Press, Boca Raton (1991).
- I. Palhan, M. Crespin, H. Estrade-Szwarckopf, and B. Rousseau. *Chem. Phys. Lett.*, 1989, **157**, 321.
- A. Tressaud, F. Moguet, S. Flandrois, M. Chambon, C. Guimon, G. Nanse, E. Papirer, V. Gupta, and O. P. Bahl. *J. Phys. Chem. Solids*, 1996, **57**, 745.
- F. Y. Xie, W. G. Xie, J. Chen, X. Liu, D. Y. Lu, and W. H. Zhang, *J. Vac. Sci. Tech. B*, 2008, **26**, 102.
- C. M. Yang, H. Kanoh, K. Kaneko, M. Yudasaka, and S. Iijima, *J. Phys. Chem. B*, 2002, **106**, 8994.

3.10 ESI-QTOF-MS Coupled to HPLC and its Application for Food Safety[32]

3.10.1 Introduction

High-performance liquid chromatography (HPLC) is a very powerful separation method widely used in environmental science, pharmaceutical industry, biological and chemical research and other fields. Generally, it can be used to purify, identify and/or quantify one or several components in a mixture simultaneously.

Mass spectrometry (MS) is a detection technique by measuring mass-to-charge ratio of ionic species. The procedure consists of different steps. First, a sample is injected in the instrument and then evaporated. Second, species in the sample are charged by certain ionized methods, such as electron ionization (EI), electrospray ionization (ESI), chemical ionization (CI), matrix-assisted laser desorption/ionization (MALDI). Finally, the ionic species wil be analyzed depending on their mass-to-charge ratio (m/z) in the analyzer, such as quadrupole, time-of-flight (TOF), ion trap and fourier transform ion cyclotron resonance.

The mass spectrometric identification is widely used together with chromatographic separation. The most common ones are gas chromatography-mass spectrometry (GC-MS) and liquid chromatography-mass spectrometry (LC-MS). Because of the high sensitivity, selectivity and relatively low price of GC-MS, it has very wide applications in drug detection, environmental analysis and so forth. For those organic chemistry research groups, it is also a daily-used and convenient equipment. However, GC-MS is ineffective if the molecules have high boiling point and/or will be decomposed at high temperature.

In this module, we will mainly talk about liquid chromatography and electrospray ionization quadrupole time-of-flight mass spectrometry (LC/ESI-QTOF-MS). As mentioned above, the LC has an efficient capacity of separation and MS has a high sensitivity and strong ability of structural characterization. Furthermore, TOF-MS, has several distinctive properties on top of regular MS, including fast acquisition rates, high accuracy in mass measurements and a large mass range. The combination of LC and ESI-TOF-MS allow us to obtain a powerful in the quantitative and qualitative analysis of molecules in complex matrices by reducing the matrix interferences. It may play an important role in the area of food safety.

3.10.2 How it works

Generally, LC-MS has four components, including an autosampler, HPLC, ionization source and mass spectrometer, as shown in Figure 3.175. Here we need to pay attention to the interface of HPLC and MS so that they can be suitable to each other and be connected. There are specified separation column for HPLC-MS, whose inner diameter (I.D.) is usually 2.0 mm. And the flow rate, which is 0.05 - 0.2 mL/min, is slower than typical HPLC. For the mobile phase, we use the combination of water and methanol and/acetonitrile. And because ions will inhibit the signals in MS, if we want to modify to mobile phase, the modifier should be volatile, such as HCO_2H, CH_3CO_2H, $[NH_4][HCO_2]$ and $[NH_4][CH_3CO_2]$.

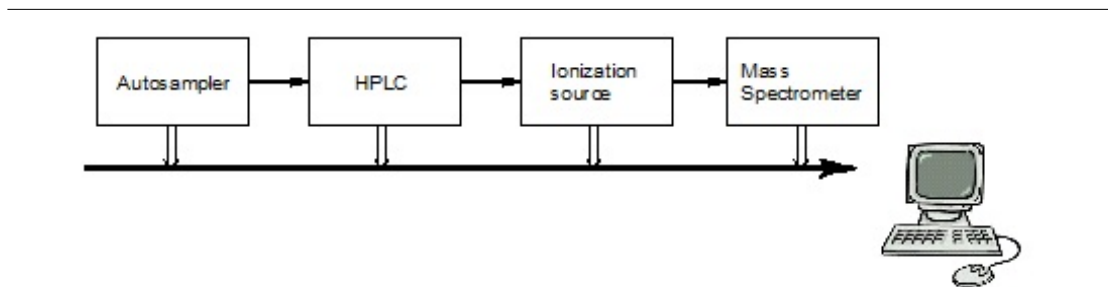[32]This content is available online at <http://cnx.org/content/m38334/1.1/>.

Figure 3.175: The component of a HPCL-MS system. Adapted from W. A . Korfmacher, *Drug Discov. Today*, 2005, **10**, 1357.

As the interface between HPLC and MS, the ionization source is also important. There are many types and ESI and atmospheric pressure chemical ionization (APCI) are the most common ones. Both of them are working at atmospheric pressure, high voltage and high temperature. In ESI, the column eluent as nebulized in high voltage field (3 - 5 kV). Then there will be very small charged droplet. Finally individual ions formed in this process and goes into mass spectrometer.

3.10.3 Comparison of ESI-QTOF-MS and other mass spectrometer methods

There are many types of mass spectrometers which can connect with the HPLC. One of the most widely-used MS systems is single quadrupole mass spectrometer, whichis not very expensive, shown in Figure 3.176. This system has two modes. One mode is *total ion monitoring* (TIM) mode which can provide the total ion chromatograph. The other is *selected ion monitoring* (SIM) mode, in which the user can choose to monitor some specific ions, and the latter's sensitivity is much higher than the former's. Further, the mass resolution of the single quadrupole mass spectrometer is 1 Da and its largest detection mass range is 30 - 3000 Da.
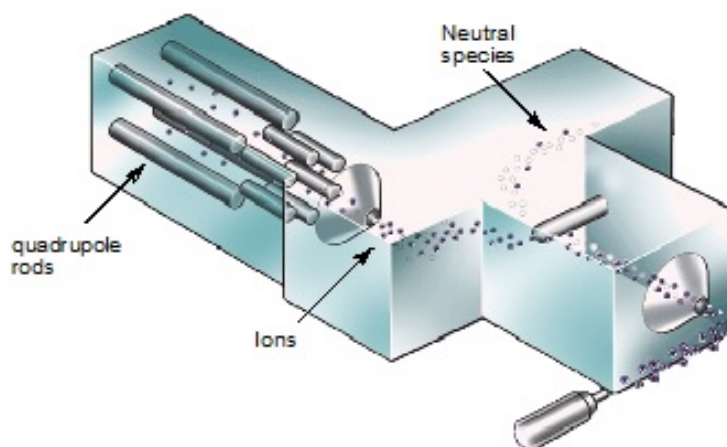
Figure 3.176: Single quadrupole mass spectrometer. Adapted from W. A. Korfmacher, *Using Mass Spectrometry for Drug Metabolism Studies*, 1st Edition, Taylor & Francis, Abingdon (2004).

The second MS system is the triple quadrupole MS-MS system, shown in Figure 3.177. Using this system, people can select the some ions, called parent ions, and use another electron beam to collide them again to get the fragment ions, called daughter ions. In other words, there are two steps to select the target molecules. So it reduces the matrix effect a lot. This system is very useful in the analysis of biological samples because biological samples always have very complex matrix; however, the mass resolution is still 1 Da.
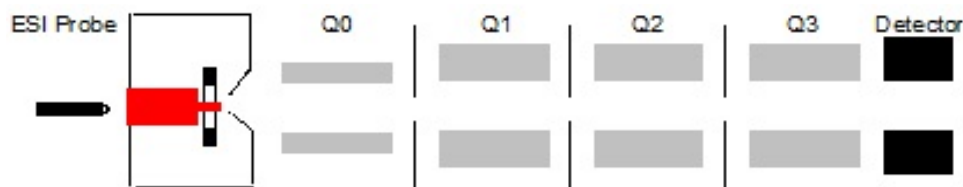

Figure 3.177: Triple quadrupole mass spectrometer. Adapted from W. A. Korfmacher, *Using Mass Spectrometry for Drug Metabolism Studies*, 1st Edition, Taylor & Francis, Abingdon (2004).

The third system is time-of-flight (TOF) MS, shown in Figure 3.178, which can provide a higher mass resolution spectrum, 3 to 4 decimals of Da. Furthermore, it can detect a very large range of mass at a very fast speed. The largest detection mass range is 20 - 10000 Da. But the price of this kind of MS is very high. The last technique is a hybrid mass spectrometer, Q-TOF MS, which combines a single quadrupole MS and a TOF MS. Using this MS, we can get high resolution chromatograph and we also can use the MS-MS system to identify the target molecules.
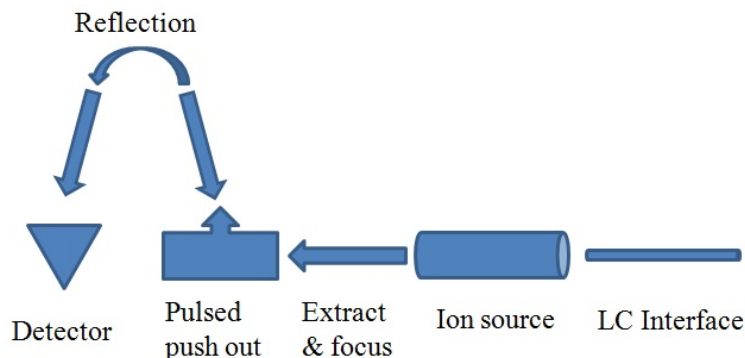
Figure 3.178: Time-of-flight mass spectrometer. Adapted from W. A. Korfmacher, *Using Mass Spectrometry for Drug Metabolism Studies*, 1st Edition, Taylor & Francis, 2004.

3.10.4 Application of LC/ESI-QTOF-MS in the detection of quinolones in edible animal food

Quinolones are a family of common antibacterial veterinary medicine which can inhibit DNA-gyrase in bacterial cells. However, the residues of quinolone in edible animal products may be directly toxic or cause resistant pathogens in humans. Therefore, sensitive methods are required to monitor such residues possibly present in different animal-producing food, such as eggs, chicken, milk and fish. The molecular structures of eight quinolones, ciprofloxacin (CIP), anofloxacin methanesulphonate (DAN), enrofloxacin (ENR), difloxacin (DIF), sarafloxacin (SARA), oxolinic, acid (OXO), flumequine (FLU), ofloxacin (OFL), are shown in Figure 3.179.
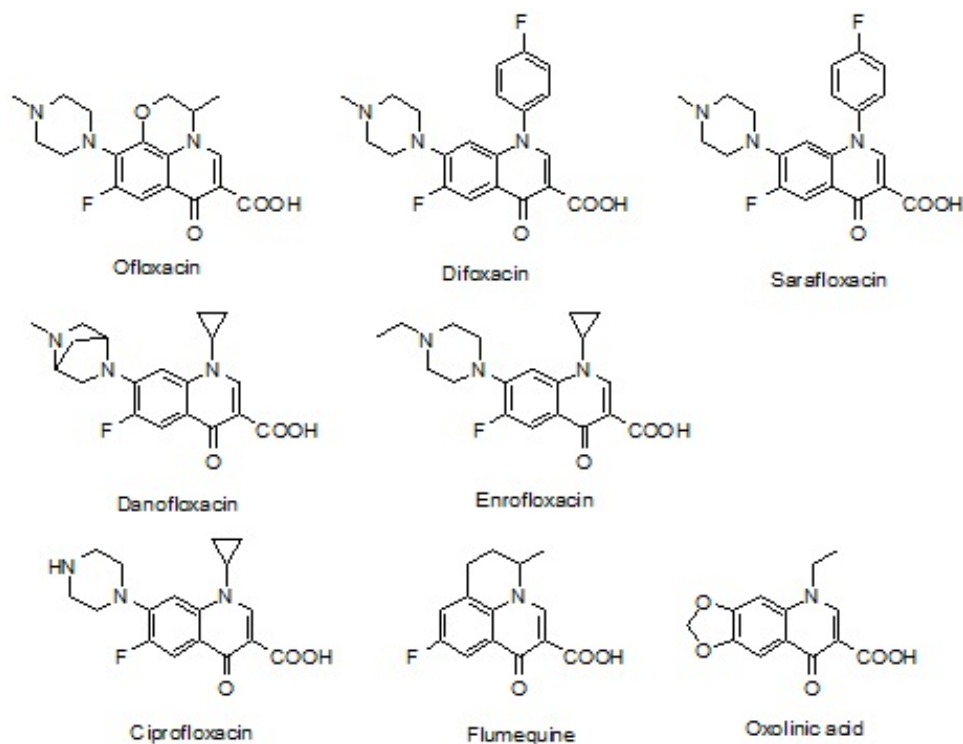
Figure 3.179: The molecular structure of eight quinolones. Adapted from M. M. Zheng, G. D. Ruan, and Y. Q. Feng, *J. Chromatogr. A*, 2009, **1216**, 7510.

LC-MS is a common detection approach in the field of food safety. But because of the complex matrix of the samples, it is always difficult to detect those target molecules of low concentration by using single quadrupole MS. The following gives an example of the application of LC/ESI-QTOF-MS.

Using a quaternary pump system, a Q-TOF-MS system, a C18 column (250 mm × 2.0 mm I.D., 5 μm) with a flow rate of 0.2 mL/min, and a mixture of solvents as the mobile phase comprising of 0.3% formic acid solution and acetonitrile. The gradient phofile for mobile phase is shown in Table 3.25. Since at acidic pH condition, the quinolones carried a positive charge, all mass spectra were acquired in the positive ion mode and summarizing 30,000 single spectra in the mass range of 100-500 Da.

Time (min)	Volume % of formic acid solution	Volume % of acetonitrile
0	80	20
12	65	35
15	20	80
20	15	85
30	15	85
30.01	80	20

Table 3.25: The gradient phofile for mobile phase.

The optimal ionization source working parameters were as follows: capillary voltage 4.5 kV; ion energy of quadrupole 5 eV/z; dry temperature 200 °C; nebulizer 1.2 bar; dry gas 6.0 L/min. During the experiments, HCO_2Na (62 Da) was used to externally calibrate the instrument. Because of the high mass accuracy of the TOF mass spectrometer, it can extremely reduce the matrix effects. Three different chromatographs are shown in Figure 3.180. The top one is the total ion chromatograph at the window range of 400 Da. It's impossible to distinguish the target molecules in this chromatograph. The middle one is at one Da resolution, which is the resolution of single quadrupole mass spectrometer. In this chromatograph, some of the molecules can be identified. But noise intensity is still very high and there are several peaks of impurities with similar mass-to-charge ratios in the chromatograph. The bottom one is at 0.01 Da resolution. It clearly shows the peaks of eight quinolones with very high signal to noise ratio. In other words, due to the fast acquisition rates and high mass accuracy, LC/TOF-MS can significantly reduce the matrix effects.
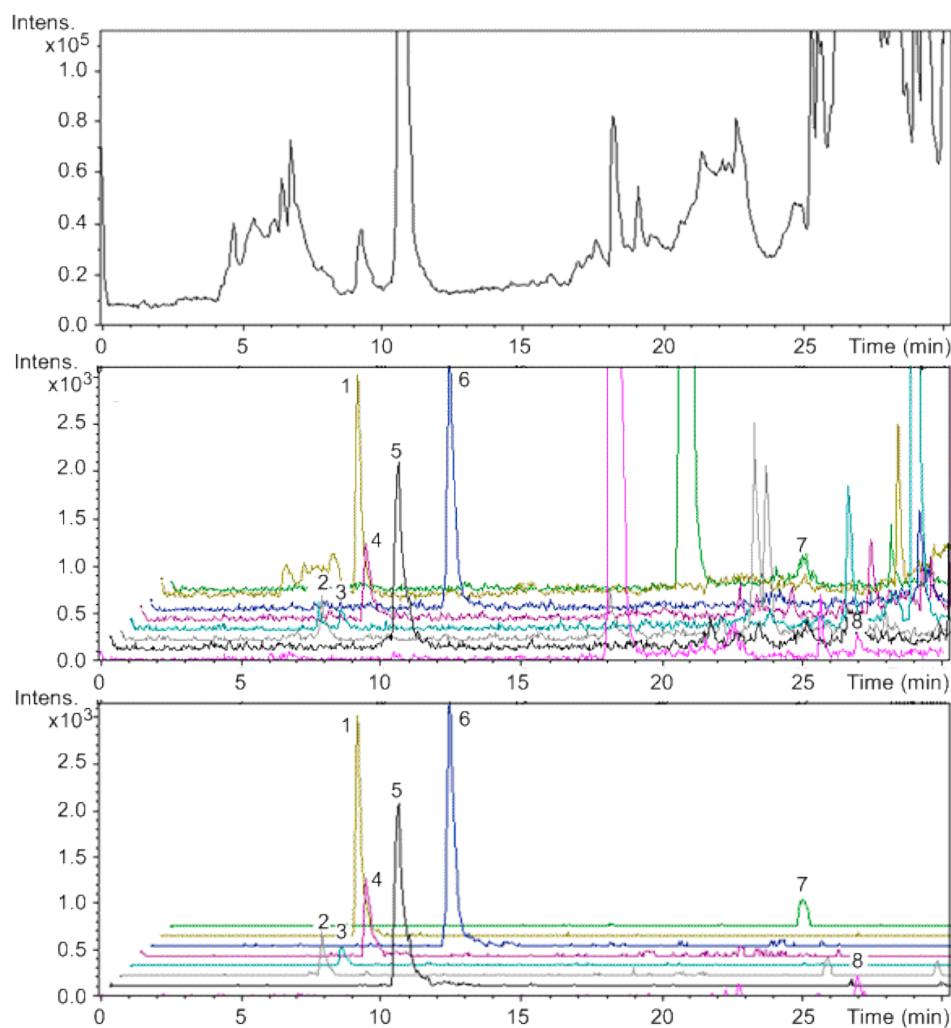
Figure 3.180: Different chromatographs of 4 ng/g eight quinolones spiked in fish samples at different mass resolutions. Peaks: 1 = OFL; 2 = CIP; 3 =DAN; 4 = ENR; 5 = SARA; 6 = DIF; 7 =OXO; 8 = FLU. Adapted from M. M. Zheng, G. D. Ruan, and Y. Q. Feng, *J. Chromatogr. A*, 2009, **1216**, 7510.

The quadrupole MS can be used to further confirm the target molecules. Figure 3.181 shows the chromatograms obtained in the confirmation of CIP (17.1 ng/g) in a positive milk sample and ENR (7.5 ng/g) in a positive fish sample. The chromatographs of parent ions are shown on the left side. On the right side, they are the characteristic daughter ion mass spectra of CIP and ENR.
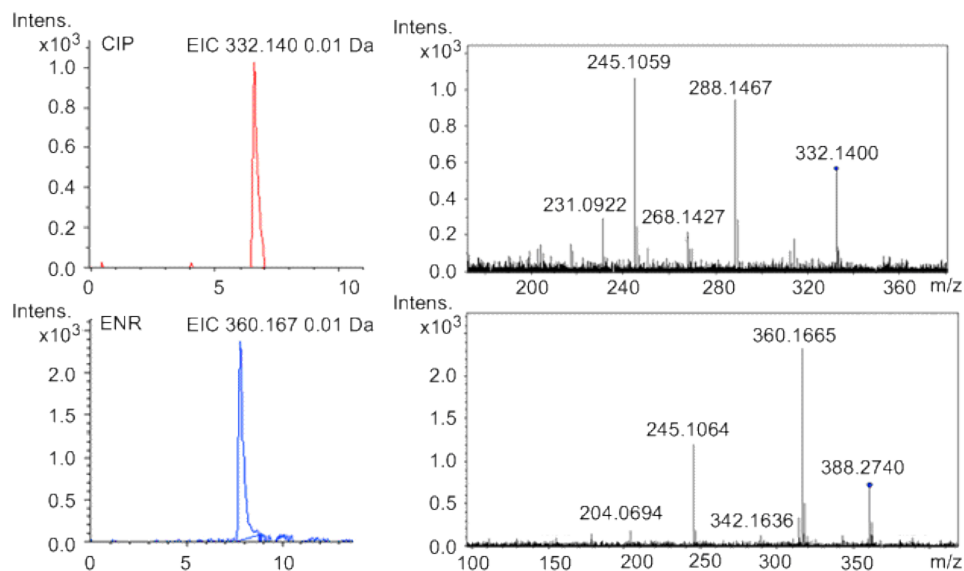
Figure 3.181: Chromatograms obtained in the confirmation of CIP (17.1 ng/g) in positive milk sample and ENR (7.5 ng/g) in positive fish sample. Adapted from M. M. Zheng, G. D. Ruan, and Y. Q. Feng, *J. Chromatogr. A*, 2009, **1216**, 7510.

3.10.5 Drawbacks of LC/Q-TOF-MS

Some of the drawbacks of LC/Q-TOF-MS are its high costs of purchase and maintenance. It is hard to apply this method in daily detection in the area of environmental protection and food safety.

In order to reduce the matrix effect and improve the detection sensitivity, people may use some sample preparation methods, such as liquid-liquid extraction (LLE), solid-phase extraction (SPE), distillation. But these methods would consume large amount of samples, organic solvent, time and efforts. Nowadays, there appear some new sample preparation methods. For example, people may use online microdialysis, supercritical fluid extraction (SFE) and pressurized liquid extraction. In the method mentioned in the Application part, we use online in-tube solid-phase microextraction (SPME), which is an excellent sample preparation technique with the features of small sample volume, simplicity solventless extraction and easy automation.

3.10.6 Bibliography

- M. S. Lee and E. H. Kerns, *Mass Spec. Rev.*, 1999, **18**, 187.
- W. A. Korfmacher, *Drug Discov. Today*, 2005, **10**, 1357.
- W. A. Korfmacher, *Using Mass Spectrometry for Drug Metabolism Studies*, 1st Edition, Taylor & Francis, Abingdon (2004).
- C. Zwiener and F. H. Frimmel, *Anal. Bioanal. Chem.*, 2004, **378**, 851.
- M. M. Zheng, G. D. Ruan, and Y. Q. Feng, *J. Chromatogr. A*, 2009, **1216**, 7510.

3.11 Mass Spectrometry

3.11.1 Principles of Mass Spectrometry and Modern Applications[33]

3.11.1.1 Introduction

Mass spectrometry (MS) is a powerful characterization technique used for the identification of a wide variety of chemical compounds. At its simplest, MS is merely a tool for determining the molecular weight of the chemical species in a sample. However, with the high resolution obtainable from modern machines, it is possible to distinguish isomers, isotopes, and even compounds with nominally identical molecular weights. Libraries of mass spectra have been compiled which allow rapid identification of most known compounds, including proteins as large as 100 kDa (100,000 amu).

Mass spectrometers separate compounds based on a property known as the mass-to-charge ratio. The sample to be identified is first ionized, and then passed through some form of magnetic field. Based on parameters such as how long it takes the molecule to travel a certain distance or the amount of deflection caused by the field, a mass can be calculated for the ion. As will be discussed later, there are a wide variety of techniques for ionizing and detecting compounds.

Limitations of MS generally stem from compounds that are not easily ionizable, or which decompose upon ionization. Geometric isomers can generally be distinguished easily, but differences in chirality are not easily resolved. Complications can also arise from samples which are not easily dissolved in common solvents.

3.11.1.2 Ionization techniques

3.11.1.2.1 Electon impact (EI)

In electon impact ionization, a vaporized sample is passed through a beam of electrons. The high energy (typically 70 eV) beam strips electrons from the sample molecules leaving a positively charged radical species. The molecular ion is typically unstable and undergoes decomposition or rearrangement to produce fragment ions. Because of this, electron impact is classified as a "hard" ionization technique. With regards to metal-containing compounds, fragments in EI will almost always contain the metal atom (i.e., $[ML_n]^{+\bullet}$ fragments to $[ML_{n-1}]^+ + L^\bullet$, not $ML_{n-1}{}^\bullet + L^+$). One of the main limitations of EI is that the sample must be volatile and thermally stable.

3.11.1.2.2 Chemical ionization (CI)

In chemical ionization, the sample is introduced to a chamber filled with excess reagent gas (such as methane). The reagent gas is ionized by electrons, forming a plasma with species such as $CH_5{}^+$, which react with the sample to form the pseudomolecular ion $[M+H]^+$. Because CI does not involve radical reactions, fragmentation of the sample is generally much lower than that of EI. CI can also be operated in negative mode (to generate anions) by using different reagent gases. For example, a mixture of CH_4 and NO_2 will generate hydroxide ions, which can abstract protons to yield the $[M-H]^-$ species. A related technique, atmospheric pressure chemical ionization (APCI) delivers the sample as a neutral spray, which is then ionized by corona discharge, producing ions in a similar manner as described above. APCI is particularly suited for low molecular weight, nonpolar species that cannot be easily analyzed by other common techniques such as ESI.

3.11.1.2.3 Field ionization/desorption

Field ionization and desorption are two closely related techniques which use quantum tunneling of electrons to generate ions. Typically, a highly positive potential is applied to an electrode with a sharp point, resulting in a high potential gradient at the tip (Figure 3.182). As the sample reaches this field, electron tunneling occurs to generate the cation, which is repelled into the mass analyzer. Field ionization utilizes gaseous samples

---

whereas in field desorption the sample is adsorbed directly onto the electrode. Both of these techniques are *soft*, resulting in low energy ions which do not easily fragment.
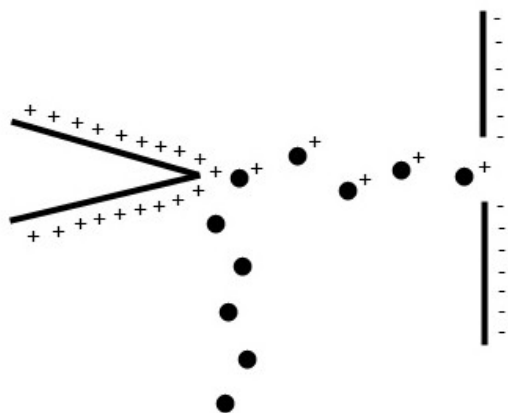

Figure 3.182: Schematic of field ionization.

3.11.1.2.4 Electrospray ionization (ESI)

In ESI, a highly charged aerosol is generated from a sample in solution. As the droplets shrink due to evaporation, the charge density increases until a *coulombic explosion* occurs, producing daughter droplets that repeat the process until individualized sample ions are generated (Figure 3.183). One of the limitations of ESI is the requirement that the sample be soluble. ESI is best applied to charged, polar, or basic compounds.
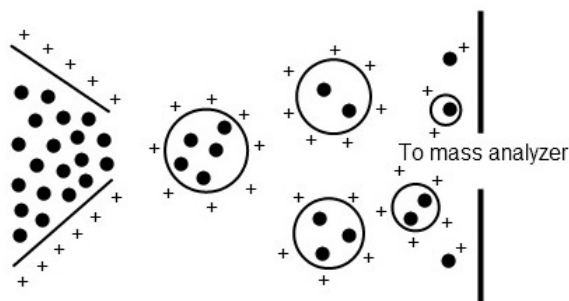

Figure 3.183: Schematic of electrospray ionization.

3.11.1.2.5 Matrix assisted laser desorption ionization (MALDI)

Laser desorption ionization generates ions by ablation from a surface using a pulsed laser. This technique is greatly improved by the addition of a matrix co-crystallized with the sample. As the sample is irradiated, a plume of desorbed molecules is generated. It is believed that ionization occurs in this plume due to a variety of chemical and physical interactions between the sample and the matrix (Figure 3.184). One of the major advantages of MALDI is that it produces singly charged ions almost exclusively and can be used to volatilize extremely high molecular weight species such as polymers and proteins. A related technique, desorption ionization on silicon (DIOS) also uses laser desorption, but the sample is immobilized on a porous silicon surface with no matrix. This allows the study of low molecular weight compounds which may be obscured by matrix peaks in conventional MALDI.
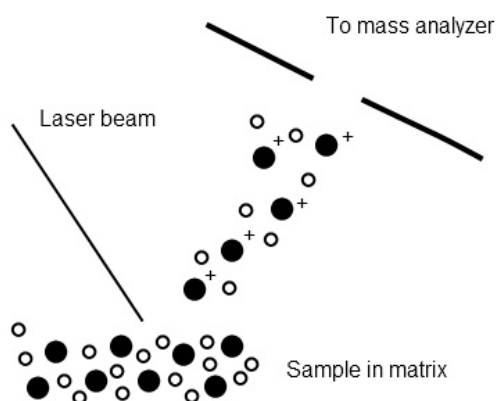
Figure 3.184: Schematic of matrix assisted laser desorption ionization.

3.11.1.2.6 Inductively coupled plasma mass spectrometry (ICP-MS)

A plasma torch generated by electromagnetic induction is used to ionize samples. Because the effective temperature of the plasma is about 10,000 °C, samples are broken down to ions of their constituent elements. Thus, all chemical information is lost, and the technique is best suited for elemental analysis. ICP-MS is typically used for analysis of trace elements.

3.11.1.2.7 Fast atom bombardment (FAB) and secondary ion mass spectrometry (SIMS)

Both of these techniques involve sputtering a sample to generate individualized ions; FAB utilizes a stream of inert gas atoms (argon or xenon) whereas SIMS uses ions such as Cs^+. Ionization occurs by charge transfer between the ions and the sample or by protonation from the matrix material (Figure 3.185). Both solid and liquid samples may be analyzed. A unique aspect of these techniques for analysis of solids is the ability to do depth profiling because of the destructive nature of the ionization technique.
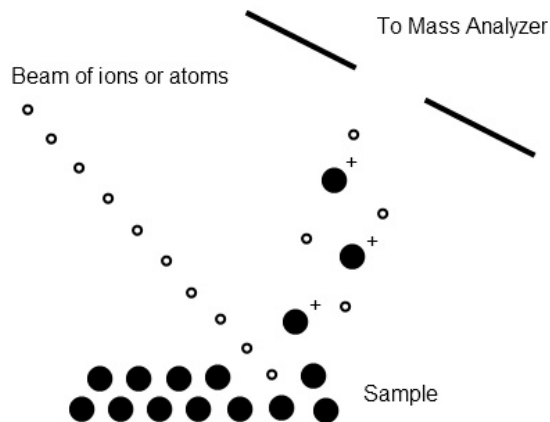
Figure 3.185: Schematic of fast atom bombardment ionization.

3.11.1.2.8 Choosing an ionization technique

Depending on the information desired from mass spectrometry analysis, different ionization techniques may be desired. For example, a hard ionization method such as electron impact may be used for a complex molecule in order to determine the component parts by fragmentation. On the other hand, a high molecular weight sample of polymer or protein may require an ionization method such as MALDI in order to be volatilized. Often, samples may be easily analyzed using multiple ionization methods, and the choice is simplified to choosing the most convenient method. For example, electrospray ionization may be easily coupled to liquid chromatography systems, as no additional sample preparation is required. Table 3.26 provides a quick guide to ionization techniques typically applied to various types of samples.

Information desired	Ionization technique
Elemental analysis	Inductively coupled plasma
Depth profiling	Fast atom bombardment/secondary ion mass spectroscopy
Chemical speciation/component analysis (fragmentation desired)	Electron impact
Molecular species identification of compounds soluble in common solvents	Electrospray ionization
	continued on next page

Molecular species identification of hydrocarbon compounds	Field ionization
Molecular species identification of high molecular weight compounds	Matrix assisted laser desorption ionization
Molecular species identification of halogen containing compounds	Chemical ionization (negative mode)

Table 3.26: Strengths of various ionization techniques.

3.11.1.3 Mass analyzers

3.11.1.3.1 Sectors

A magnetic or electric field is used to deflect ions into curved trajectories depending on the m/z ratio, with heavier ions experiencing less deflection (Figure 3.186). Ions are brought into focus at the detector slit by varying the field strength; a mass spectrum is generated by scanning field strengths linearly or exponentially. Sector mass analyzers have high resolution and sensitivity, and can detect high mass ranges, but are expensive, require large amounts of space, and are incompatible with the most popular ionization techniques MALDI and ESI.
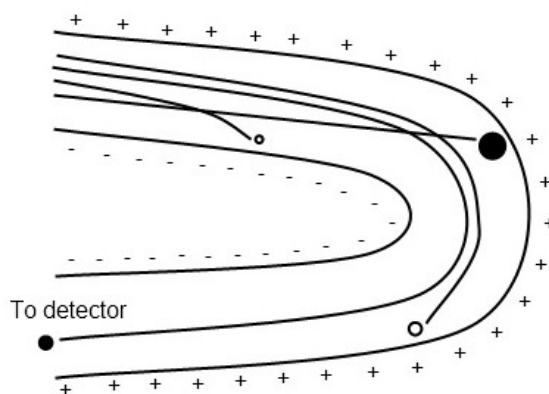

Figure 3.186: Schematic of a magnetic sector mass analyzer.

3.11.1.3.2 Time-of-flight (TOF)

The amount of time required for an ion to travel a known distance is measured (Figure 3.187). A pulse of ions is accelerated through and electric analyzer such that they have identical kinetic energies. As a result, their velocity is directly dependent on their mass. Extremely high vacuum conditions are required to extend the mean free path of ions and avoid collisions. TOF mass analyzers are fastest, have unlimited mass ranges, and allow simultaneous detection of all species, but are best coupled with pulsed ionization sources such as MALDI.
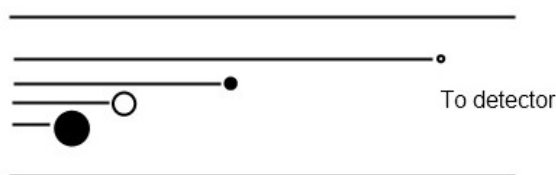
Figure 3.187: Schematic of a time-of-flight (TOF) mass analyzer.

3.11.1.3.3 Quadrupole

Ions are passed through four parallel rods which apply a varying voltage and radiofrequency potential (Figure 3.188). As the field changes, ions respond by undergoing complex trajectories. Depending on the applied voltage and RF frequencies, only ions of a certain m/z ratio will have stable trajectories and pass through the analyzer. All other ions will be lost by collision with the rods. Quadrupole analyzers are relatively inexpensive, but have limited resolution and low mass range.
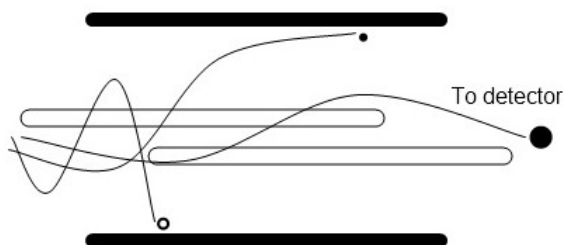

Figure 3.188: Schematic of a quadrupole mass analyzer.

3.11.1.3.4 Ion trap

Ion traps operate under the same principle as quadrupole, but contain the ions in space. Electrodes can be manipulated to selectively eject ions of desired m/z ratios, allowing for mass analysis. Ion traps are uniquely suited for repeated cycles of mass spectrometry because of their ability to retain ions of desired m/z ratios. Selected fragments can be further fragmented by collision induced dissociation with helium gas. Ion traps are compact, relatively inexpensive, and can be adapted to many hybrid instruments.

3.11.1.4 Coupling mass spectrometry to other instruments

Mass spectrometry is a powerful tool for identification of compounds, and is frequently combined with separation techniques such as liquid or gas chromatography for rapid identification of the compounds within

a mixture. Typically, liquid chromatography systems are paired with ESI-quadrupole mass spectrometers to take advantage of the solvated sample. GC-MS systems usually employ electron impact ionization and quadrupole or ion trap mass analyzers to take advantage of the gas-phase molecules and fragmentation libraries associated with EI for rapid identification.

Mass spectrometers are also often coupled in tandem to form MS-MS systems. Typically the first spectrometer utilizes a hard ionization technique to fragment the sample. The fragments are passed on to a second mass analyzer where they may be further fragmented and analyzed. This technique is particularly important for studying large, complex molecules such as proteins.

3.11.1.5 Bibliography

- W. Henderson and J. S. McIndoe, *Mass Spectrometry of Inorganic, Coordination, and Organometallic Compounds*, John Wiley & Sons Ltd., Chichester (2005).
- *Inorganic Mass Spectrometry Fundamentals and Applications*, Ed. C. M. Barshick, D. C. Duckworth, and D. H. Smith, Marcel Dekker Inc., New York (2000).
- F. W. McLafferty, *Science*, 1981, **214**, 280.

Solutions to Exercises in Chapter 3

Solution to Exercise 3.7.3.1 (p. 339)
Using frequency data:
Frequency of peak f - frequency of peak g = 74.82 Hz − 67.76 Hz = 7.06 Hz
Frequency of peak e - frequency of peak f = 81.88 Hz − 74.82 Hz = 7.06 Hz
Average = 7.06 Hz
∴ J(H-H) = 7.06 Hz

Alternatively, using chemical shift data:
Chemical shift of peak f - chemical shift of peak g = 1.2470 ppm − 1.1293 ppm = 0.1177 ppm
Chemical shift of peak e - chemical shift of peak f = 1.3646 ppm − 1.2470 ppm = 0.1176 ppm
Average = 0.11765 ppm
0.11765 ppm x 60 MHz = 7.059 Hz
∴ J(H-H) = 7.06 Hz

Notice the coupling constant for this multiplet is the same as that in the example. This is to be expected since the two multiplets are coupled with each other.